SEL-64-025

BISTATIC-RADAR METHODS FOR STUDYING PLANETARY IONOSPHERES AND SURFACES

by

Gunnar Fjeldbo

April 1964

Final Report

Prepared under

National Science Foundation
Grant NSF G-21543

Scientific Report No. 2

Prepared under
National Aeronautics and Space Administration
Research Grant No. NsG-377

Radioscience Laboratory
Stanford Electronics Laboratories
Stanford University Stanford, California

Abstract

The transmission of radio waves from the earth to a receiver in a spacecraft that is moving behind a planet makes it possible to observe the variations in the amplitude, phase path, or group path caused by the planetary ionosphere. It is shown that measurement of any one of these quantities may be used to determine the radial electron density distribution in that part of the planetary ionosphere which is probed by the signal. Measurement of two of these quantities simultaneously will reduce uncertainties due to changes in the interplanetary medium or the earth's ionosphere during the experiment. Separate radial electron density distributions can be obtained from the measurements during immersion and emersion and these are related to the spatial properties of the atmosphere on the planet. It is shown that the lower atmosphere as well as the ionosphere of a planet can be studied by using so high a frequency that the signal is not influenced by the ionized component of the atmosphere.

It is also shown that the statistical properties of a signal reflected from a planetary surface can be related to the surface statistics when the surface roughness scale is larger than the wavelength. A relation is found between the surface-autocorrelation function and the time-autocorrelation function of the reflected signal, a generalization of results obtained previously for monostatic radar. When a circularly polarized wave is transmitted, it is shown that the mean value of the dielectric constant and the conductivity for the planetary surface may be found from the shape and orientation of the polarization ellipse for the reflected signal.

CONTENTS

ILLUSTRATIONS

ACKNOWLEDGMENT

The author wishes to express his appreciation for the encouragement and advice given by the supervisors of this research, Professors L. A. Manning and Von R. Eshleman.

The research reported in this paper was supported by the National Science Foundation, the National Aeronautics and Space Administration, and the Office of Naval Research.

I. INTRODUCTION

Ground-based radar equipment is being used to study the moon and the closest planets. However, there are severe limitations associated with having both the transmitter and the receiver on the earth. These limitations can now be overcome, however, since it has become possible in recent years to send equipment to the moon and the closest planets.

In the following chapters techniques are studied for exploring the moon and the planets using bistatic radar. Bistatic radar differs from monostatic radar in that the transmitter and the receiver are situated at different locations.

One can transmit radio waves from the earth and receive them in a spacecraft moving behind a planet. If the planet is surrounded by an ionosphere, the signal will be influenced during the occultation. The changes in the signal due to the planetary ionosphere can be used to determine the electron density distribution and possibly some other interesting properties of the planetary ionosphere. The solution of this problem is presented in two steps. First, the changes in the signal are found in terms of the electron density profile of the planetary ionosphere (Chapter II). Later (in Chapter V) the problem is reversed and it is shown how the electron density distribution can be determined.

More specifically, Chapter II is used to develop high-frequency approximations (transmitter frequency much higher than the maximum plasma frequency in the planetary ionosphere) for amplitude, phase, etc., for the waves received behind a planetary ionosphere with known electron density distribution. Why the high-frequency case is of such importance will become clear at the end of the study.

The results derived in Chapter II are applied to the exponential and the Chapman ionospheric model in Chapters III and IV, respectively. The results are represented graphically in a normalized form so that they can be easily used when the exponential or the Chapman model applies. It is also shown that more complex ionospheres can be studied by considering them as being constructed from a combination of these basic models.

Chapter V is mainly devoted to the development of processes that can be used to determine the radial electron density distribution in that part of the planetary ionosphere which is probed by the signal. It is shown that measurement of either the amplitude, the phase path, or the group path during the occultation can be used to determine the electron density profile.

Radio waves reflected from the planetary surface will also be received in the spacecraft while it is in the vicinity of the planet. It is, of course, necessary to be able to distinguish between the direct and the reflected signal. Chapter VI shows that this is possible, and it also shows that the reflected signal may be used to determine statistical properties of the planetary surface, such as roughness-autocorrelation function, mean dielectric constant, etc.

II. PROPAGATION OF HIGH-FREQUENCY RADIO WAVES IN PLANETARY IONOSPHERES WITH KNOWN ELECTRON DENSITY DISTRIBUTION

This chapter is devoted mainly to the study of amplitude, and of the phase and group paths for waves refracted in a planetary ionosphere with a known electron density profile.

Later (in Chapter V) the problem is reversed in order to determine what can be learned about the ionosphere when the properties of the transmitted and the received waves are known. This is analogous to the circuit engineering problem of finding the two-port network equivalent when input and output are given.

We will assume that a circularly polarized wave is transmitted from the earth and that the transmitted frequencies lie well above the maximum plasma critical frequency, both for the earth's ionosphere and for the planetary ionosphere to be explored. Under these conditions the magnetoionic theory shows that the effect of magnetic fields on amplitude and phase can be neglected.

The results derived for phase path and amplitude are also valid when a linearly polarized wave is transmitted from the earth. In the latter case one can also observe Faraday rotation. Assuming that the Faraday rotation due to variations in the earth's ionosphere can be neglected or subtracted out, transmitting linearly polarized waves yields a means of exploring the planetary magnetic field (if there is any). This problem is discussed later.

The geometry is illustrated in Fig. 1. That part of the trajectory along which occultation can be observed may often be well approximated with a straight line. The y axis goes through the center of the planet and the transmitter on the earth. The x-y plane is chosen parallel to the fly-by trajectory.

For a spherically symmetric ionosphere, it is convenient to rotate the points along the trajectory around the y axis until they end up in the x-y plane. In this way a new curve, which here will be called the equivalent trajectory, is obtained in the x-y plane. In the spherically symmetric case, it is sufficient to study the phase and amplitude of the waves in the x-y plane, which will then also give phase path and amplitude along the true trajectory.

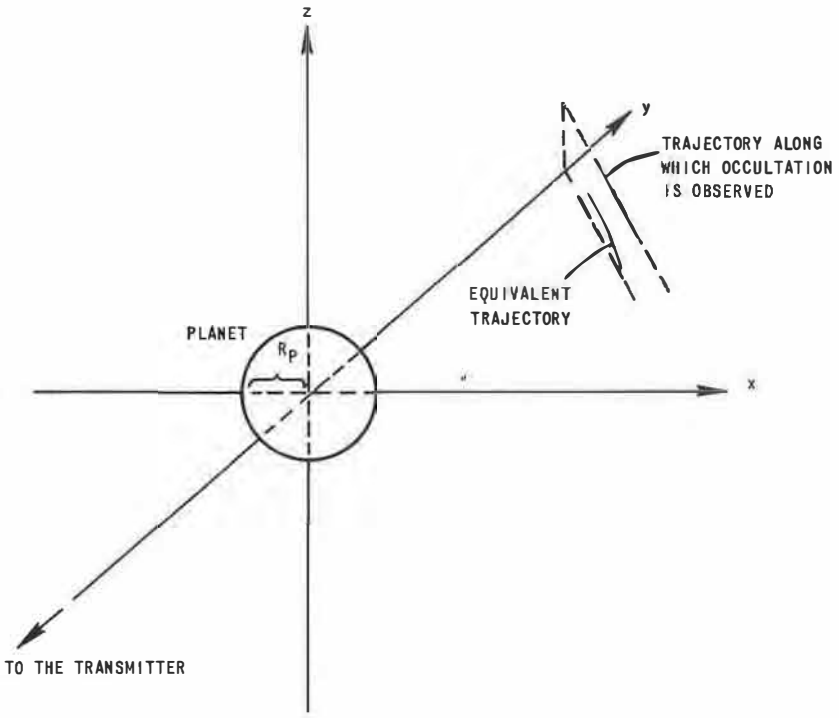

FIG. 1. GEOMETRY DURING THE OCCULTATION.

In the following sections the ray theory is applied to analyze the propagation through the planetary ionosphere. The refracting medium is inhomogeneous but isotropic. The energy is therefore propagating along the wave normal and this direction can be found from Snell's Law.

Necessary corrections to the ray-theory solution are taken up later.

A. RAYPATHS

Refraction in spherically symmetric ionospheres is discussed first because the effect of nonspherical perturbations in the electron density distribution is small. A polar coordinate system can be used to describe the raypaths in the x-y plane when the ionosphere is assumed spherically symmetric.

The differential equation for the raypaths can be derived in the following way. From the triangle ABC in Fig. 2 it is seen that

$$r \frac{d\phi}{dr} = \tan i \tag{2.1}$$

To obtain an explicit expression for the rays in terms of r and ϕ, a relation between i and the refractive index $\mu(r)$ is needed. It is seen from Fig. 3 that for an ionosphere built up of shells (spherical layers) with constant μ, one has

$$r_1 \sin i_1 = r_2 \sin \gamma_2 \qquad \text{(law of sines)}$$

$$\mu_1 \sin \gamma_2 = \mu_2 \sin i_2 \qquad \text{(Snell's Law)}$$

$$r_2 \sin i_2 = r_3 \sin \gamma_3 \qquad \text{(law of sines)}$$

$$\vdots$$

$$\mu_{n-1} \sin \gamma_n = \mu_n \sin i_n \qquad \text{(Snell's Law)}$$

The product of these equations gives

$$\mu_1 r_1 \sin i_1 = \mu_n r_n \sin i_n$$

or when $\mu(r)$ is a continuous function of r,

$$\mu r \sin i = \mu_o r_o = a \tag{2.2}$$

where r_o is the radius of closest approach for the raypath and μ_o is the refractive index at this point. The distance between the center of the planet and the raypath asymptote is denoted by a. Equation (2.2) is sometimes called Bouguer's rule.

Combining Eqs. (2.1) and (2.2) yields the differential equation for the raypath

$$\frac{d\phi}{dr} = \frac{1}{r}\left[\left(\frac{r\mu}{r_o\mu_o}\right)^2 - 1\right]^{-1/2} \tag{2.3}$$

This is a fairly well known result [Ref. 1].

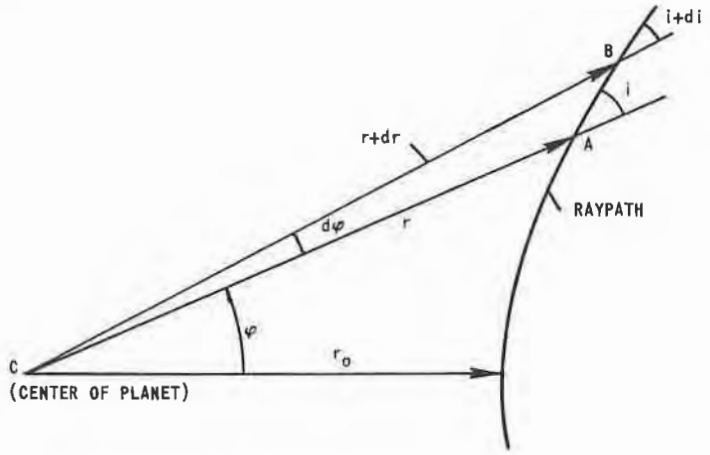

FIG. 2. RAYPATH GEOMETRY.

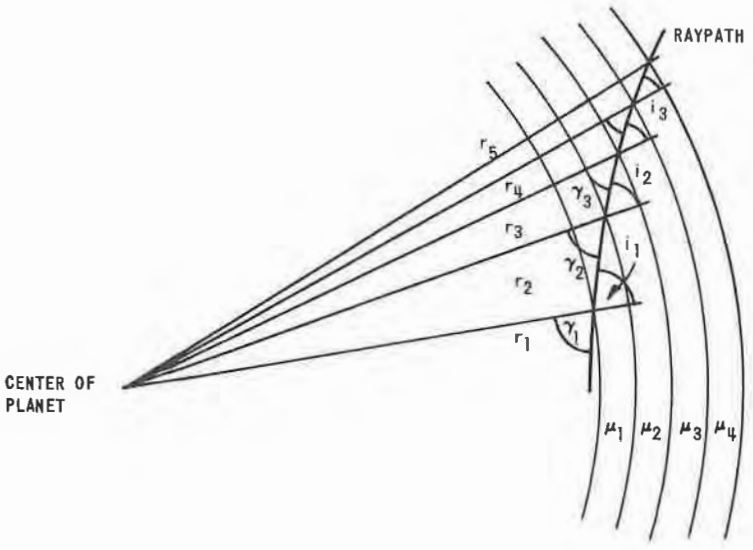

FIG. 3. REFRACTION OF RAYPATH BY CONCENTRIC SPHERICAL LAYERS.

Assuming that the effects of the magnetic field and the collisions are negligible, we get from the magnetoionic theory

$$\mu^2(r) = 1 - X(r) \tag{2.4}$$

where

$$X(r) = \frac{80.6}{f^2} N(r) \tag{2.5}$$

Here, f is the frequency and $N(r)$ is the radial distribution of electron density in the planetary ionosphere.

By combining Eq. (2.3) and Eq. (2.4) and integrating, one obtains

$$\phi = \int_{r_o}^{r} \frac{1}{r} \left[\left(\frac{r}{r_o} \right)^2 \frac{1 - X(r)}{1 - X(r_o)} - 1 \right]^{-1/2} dr \tag{2.6}$$

where $\phi = o$ for $r = r_o$.

Assuming that the electron density profile is known, one can use Eq. (2.6) to determine raypaths for different r_o. This family of raypaths (Fig. 4) may be used to find the ray pictures when some radiating source is present inside or outside the ionosphere. For instance, when the source is far away from the planet, all the rays should be rotated about the origin so that one of their asymptotes points towards the source.

In most fly-by experiments, it is expected that the trajectory will lie well outside the ionosphere, and this makes it possible to simplify the procedure. Instead of finding the total raypath, it is sufficient to determine the asymptotes. The geometry is shown in Fig. 5 where:

$$\phi_m = \frac{\pi}{2} - \psi = \int_{r_o}^{\infty} \frac{1}{r} \left[\left(\frac{r}{r_o} \right)^2 \frac{1 - X(r)}{1 - X(r_o)} - 1 \right]^{-1/2} dr \tag{2.7}$$

and

$$q = \frac{a}{\cos(2\psi + \beta)} - R_p \tag{2.8}$$

The new geometrical quantities involved are shown in Fig. 5.

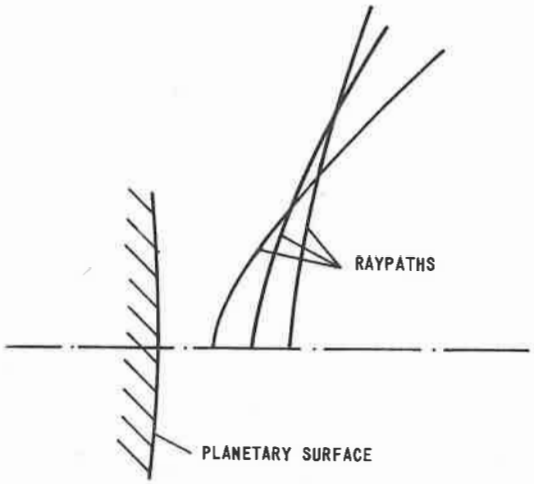

FIG. 4. FAMILY OF RAYPATHS.

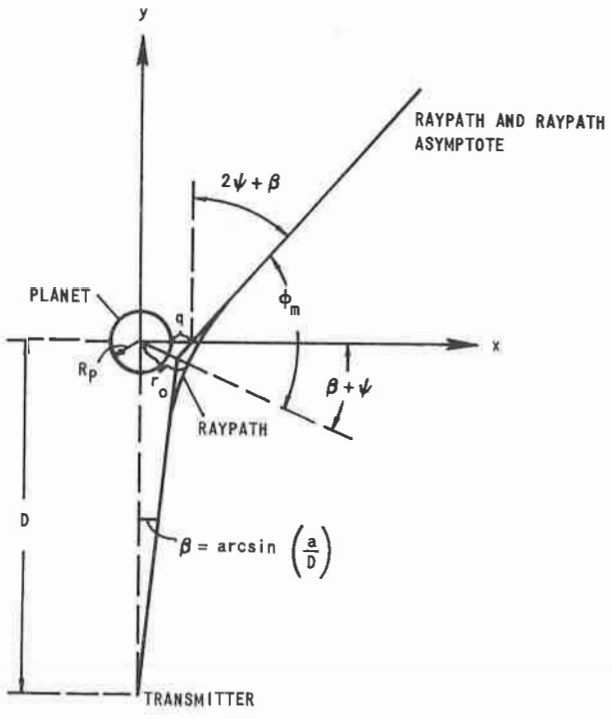

FIG. 5. IMPORTANT RAYPATH PARAMETERS.

We will now introduce a new variable α given by

$$\alpha = \arccos\left(\frac{r_o}{r}\right) \tag{2.9}$$

Now one obtains for the total angle (2ψ) that the rays are refracted:

$$2\psi = 2\int_o^{\pi/2} \left\{ 1 - \left[\frac{1 - X(r_o)}{1 + \dfrac{X(r_o)\cos^2\alpha - X(r_o/\cos\alpha)}{\sin^2\alpha}} \right]^{1/2} \right\} d\alpha \tag{2.10}$$

This equation is correct for a wide range of frequencies as long as collisions and magnetic fields are absent. However, we are mainly interested in the high-frequency case $(X \ll 1)$, and it would be desirable to simplify Eq. (2.10). Looking at

$$\delta(\alpha, r_o) = X(r_o) \frac{\cos^2\alpha - \dfrac{X(r_o/\cos\alpha)}{X(r_o)}}{\sin^2\alpha} \tag{2.11}$$

one sees that $|\delta|$ is less than 1 for α greater than 0 because $X(r_o) \ll 1$. For $|\alpha| \ll 1$ we have

$$X\left(\frac{r_o}{\cos\alpha}\right) = X(r_o) + \frac{r_o}{2}\alpha^2 X'(r_o) + \ldots$$

Thus for small α:

$$\delta(\alpha, r_o) = -X(r_o)\left[1 + \frac{r_o}{2}\frac{X'(r_o)}{X(r_o)}\right]$$

which also turns out to be small compared to 1 for the ionospheric models we will consider. Using this, we can expand the integrand in Eq. (2.10) and, maintaining only the first-order terms in X, we obtain:

$$2\psi = X(r_o)\int_o^{\pi/2} \frac{1 - \dfrac{X(r_o/\cos\alpha)}{X(r_o)}}{\sin^2\alpha}\, d\alpha \tag{2.12}$$

when $|\delta(\alpha, r_o)| \ll 1$.

For the cases we shall consider, 2ψ turns out to be less than 1 or 2 deg, and Eq. (2.12) usually provides good accuracy.

Equation (2.12) shows that there is a linear relation between 2ψ and X. If we have an ionospheric model $[X(r_o/\cos\alpha)]$ built up of several layers $[X_\nu (r_o/\cos\alpha)]$, this can be written

$$X\left(\frac{r_o}{\cos\alpha}\right) = \sum_\nu X_\nu \left(\frac{r_o}{\cos\alpha}\right) \tag{2.13}$$

Applying Eq. (2.12), we find for the refracted angle:

$$2\psi = \sum_\nu 2\psi_\nu \tag{2.14}$$

where $2\psi_\nu$ is caused by the ν^{th} layer, etc. In other words, superposition applies, and refraction due to each layer may be treated as if it were the only layer present.

In Chapters III and IV, exponential and Chapman-distributed electron density profiles are assumed. More complex ionospheres can be studied by considering them as being constructed from a combination of these basic models.

We have so far assumed a spherically symmetric ionosphere and, on this basis, determined the raypath. However, one can also start by assuming an ionosphere with nonspherical perturbations. Let us look at the wavefronts as a wave propagates through a planetary ionosphere for the high-frequency case illustrated in Fig. 6. The wavefronts become slightly perturbed as the wave propagates through the ionosphere. The phase at point P in Fig. 6 is proportional to the integral of μ along the raypath. For the case shown, it does not matter whether one integrates μ along the raypath or along the straight line ℓ. (This is only true when the point P is close behind the ionosphere and when the refraction is small.) Using this argument, we see that $\int(1 - \mu)\, dy$ taken along ℓ gives the perturbation on the wavefront in the y direction.

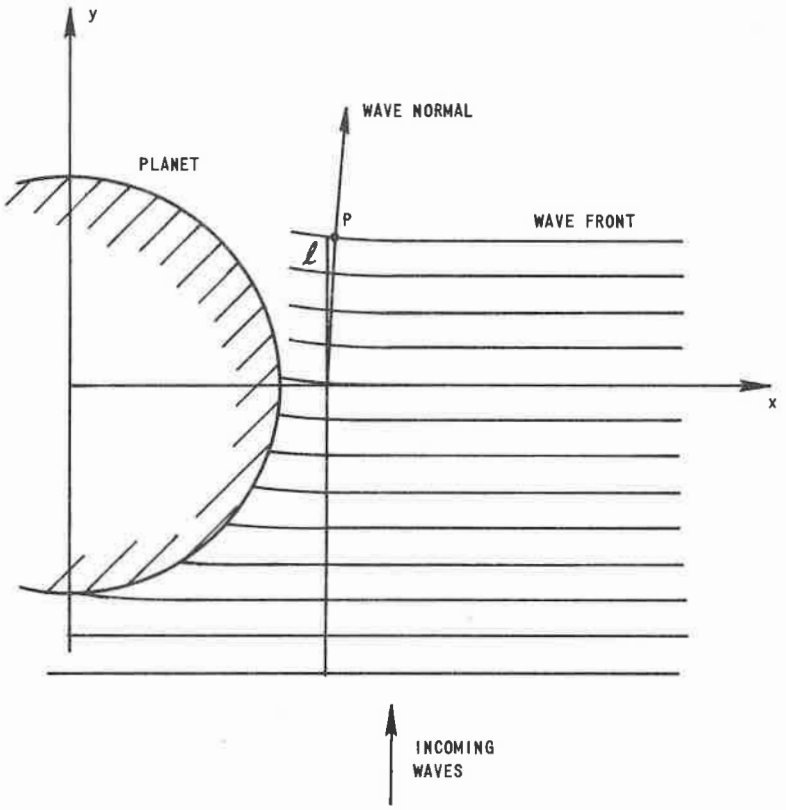

FIG. 6. PERTURBATION OF THE WAVEFRONTS.

The angle the wave normal makes with the y axis (2ψ) is equal to minus the slope of the wavefront, and we therefore obtain:

$$2\psi = \frac{d}{dx} \int_{\substack{\text{through} \\ \text{the} \\ \text{medium}}} \mu \, dy \qquad (2.15)$$

where the gradient in μ is assumed negligible perpendicular to the x-y plane.

Equation (2.15) states that the angular deviation of the rays in the high-frequency case is equal to the gradient in the integrated phase refractive index, μ. This result has, for instance, been used to

determine horizontal gradients in the total ionization of the earth's ionosphere by measuring the ionospheric refraction of waves from radio stars [Ref. 2].

Let us apply Eq. (2.15) to the spherically symmetric case and compare this with the results we obtained previously. Equation (2.4) gives in the high-frequency case:

$$\mu(r) = 1 - \frac{1}{2} X(r) \tag{2.16}$$

thus

$$\int \mu \, dy = \int dy - \frac{1}{2} \int X(r) \, dy$$

and

$$2\psi = - \frac{1}{2} \frac{d}{dx} \int_{-\infty}^{+\infty} X(r) \, dy$$

After introducing $x = r_o$ and $y = r_o \tan \alpha$, we obtain:

$$2\psi = - \frac{d}{dr_o} \int_o^{\pi/2} X\left(\frac{r_o}{\cos \alpha}\right) \frac{r_o}{\cos^2 \alpha} \, d\alpha = - \int_o^{\pi/2} \frac{X(r_o/\cos \alpha)}{\cos^2 \alpha} \, d\alpha$$

$$- \int_o^{\pi/2} X'\left(\frac{r_o}{\cos \alpha}\right) \frac{r_o \, d\alpha}{\cos^3 \alpha}$$

The last integral can be integrated by parts giving

$$2\psi = - \int_o^{\pi/2} \frac{X(r_o/\cos \alpha)}{\cos^2 \alpha} \, d\alpha + \int_o^{\pi/2} X\left(\frac{r_o}{\cos \alpha}\right)\left(\frac{1}{\cos^2 \alpha} - \frac{1}{\sin^2 \alpha}\right) d\alpha$$

$$+ X(r_o) \lim_{\alpha \to 0} \left(\frac{1}{\sin \alpha \cos \alpha}\right)$$

Further manipulations give

$$2\psi = \int_o^{\pi/2} \frac{X(r_o) - X(r_o/\cos \alpha)}{\sin^2 \alpha} \, d\alpha + X(r_o) \lim_{\alpha \to 0} \left(\frac{1}{\sin \alpha \cos \alpha} - \cot \alpha\right)$$

where the limit is zero. By comparing this expression with Eq. (2.12), we see that the two approaches yield the same result, and we have therefore justified the simple arguments leading to Eq. (2.15).

We have so far limited the discussion to refraction caused by gradients in the ionization. However, it is worthwhile noting that the same results can be used to treat refraction in the lower atmosphere. For the refraction index in this case, we can use [Ref. 3]:

$$\mu = 1 + 10^{-6}\left(\frac{79P}{T} + \frac{380,000e}{T^2}\right) \tag{2.17}$$

where P is the partial pressure of dry air in millibars, e is the partial pressure of water vapor in millibars, and T is the temperature in degrees Kelvin. This corresponds to replacing Eq. (2.5) by

$$X = -2\cdot 10^{-6}\left(\frac{79P}{T} + \frac{380,000e}{T^2}\right) \tag{2.18}$$

When T is constant throughout the atmosphere, the pressure can be expressed as an exponential function of height. We can therefore use Chapter III to take into account the influence of the atmosphere.

B. PHASE PATH (s_p) AND GROUP PATH (s_g)

The ray picture is useful in the visualization of the propagation, but we are more interested in those quantities which can be measured, such as phase and group paths. The phase path of the signal is found by integrating the phase refractive index μ along the raypath from the transmitter (or some reference surface), through the planetary ionosphere and to the receiver.

There are two reasons why the phase path changes as the transmitter is occulted by the ionosphere:

1. The electrons advance the phase and therefore tend to make the phase path shorter.
2. The raypaths are curved due to refraction and this tends to increase the phase path.

It is necessary to study both these competing effects in order to draw any conclusions about how the phase path is changing.

Previously we indicated that the phase path could be found by integrating μ along the raypath. This method is sufficient when the propagation takes place over relatively short distances, such as between two points on the earth's surface. However, it is not a practical approach in our case because for most fly-by trajectories, one has to integrate over such huge distances that the effect of the planetary ionosphere more or less disappears. One can improve the accuracy, when a digital computer is available, by using double-precision arithmetic. However, since the use of double-precision arithmetic slows down the execution of the program considerably, it is not a very attractive solution from an economical point of view. Hence, it is desirable to look for a more sophisticated method for the calculation of the phase path.

Our primary interest is not so much the total phase path itself, but rather the changes in the phase path due to the planetary ionosphere. These changes would be fairly simple to compute if the raypaths were the same with and without the ionosphere. In the latter case, it would only be necessary to integrate the electron density along straight lines. However, we must look deeper into this because the rays are curved.

Defining s_p as the <u>decrease</u> in the phase path due to the presence of the planetary ionosphere, we can write:

$$s_p = \frac{f}{c}\left(\int_{\substack{\text{along}\\ \text{straight}\\ \text{line}}} ds - \int_{\substack{\text{along}\\ \text{raypath}}} \mu \, ds \right) \qquad (2.19)$$

where the second integral is taken along the actual raypath, and the first integral is taken along the raypath connecting transmitter and receiver when the planetary ionosphere is (imagined) removed. The parameter c is the free-space phase velocity and f is the frequency. Thus, s_p gives the phase difference in cycles.

In the high-frequency case, Eq. (2.19) gives

$$\frac{f}{c}\left(\int_{\substack{\text{along}\\ \text{straight}\\ \text{line}}} ds - \int_{\substack{\text{along}\\ \text{raypath}}} ds + \frac{1}{2} \int_{\substack{\text{along}\\ \text{raypath}}} X\, ds \right) = s_p = - s_1 + s_2 \qquad (2.20)$$

where

$$s_1 = \frac{f}{c}\left(\int_{\substack{\text{along}\\ \text{raypath}}} ds - \int_{\substack{\text{along}\\ \text{straight}\\ \text{line}}} ds \right) \qquad (2.21)$$

$$s_2 = \frac{f}{2c} \int_{\substack{\text{along}\\ \text{raypath}}} X\, ds \qquad (2.22)$$

The group path is of interest when one transmits pulses instead of cw. For the <u>increase</u> in group path (s_g) due to the presence of the planetary ionosphere, one obtains

$$s_g = s_1 + s_2 \qquad (2.23)$$

when magnetic fields and collisions can be neglected. The group time delay due to the planetary ionosphere is (s_g/f) with this notation.

Equation (2.21) gives s_1 in terms of two integrals; the magnitude of these integrals is very large compared to their difference. It is therefore not practical, as described earlier, to compute the two integrals and then subtract them. Instead, one can compute s_1 in two steps. The first step consists of finding s_1 as if the propagation was along the raypath asymptotes. The actual raypath between the transmitter and the receiver may be shorter or longer than the distance measured along the raypath asymptotes, and it is the purpose of the second step to correct for this difference (Δs_1).

One obtains, when the rays can be considered parallel before they enter the planetary ionosphere:

$$s_1 = \frac{f}{c} (x - a) \tan \psi + \Delta s_1 \qquad (2.24)$$

where x designates the x-coordinate of the receiver for the equivalent trajectory, and a and ψ are given by Eq. (2.2) and Eq. (2.12), respectively.

Computation of Δs_1 requires integration. Use of a polar coordinate system to find Δs_1 is not practical because the errors get larger as the distance to the planetary center is increased and the process does, for this reason, not converge. Figure 7 shows a more convenient coordinate system giving fast convergence when ξ is used as a dummy variable of integration. It turns out that Δs_1 represents a higher order correction to s_1 and can often be neglected, as later results will show.

The phase advance or group delay due to the electrons is given by Eq. (2.22). Again using the polar coordinate system and α as a dummy variable, we obtain:

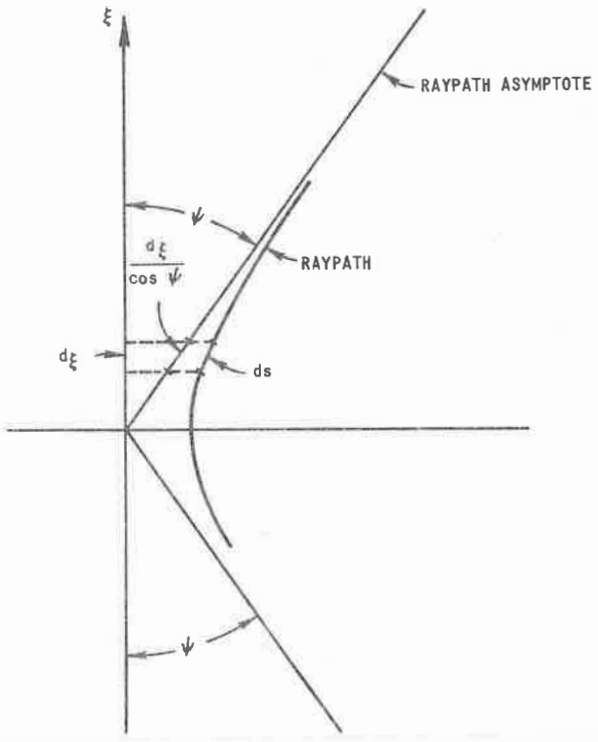

FIG. 7. A CONVENIENT COORDINATE SYSTEM FOR CALCULATION OF Δs_1.

$$s_2 = \frac{f}{c} r_o \int_o^{\pi/2} \frac{X(r_o/\cos\alpha)}{\cos^2\alpha} \left[\sin^2\alpha + \cos^2\alpha \left(\frac{d\phi}{d\alpha}\right)^2\right]^{1/2} d\alpha \qquad (2.25)$$

where

$$\left(\frac{d\phi}{d\alpha}\right)^2 = [1 - X(r_o)] \left[1 + \frac{X(r_o)\cos^2\alpha - X(r_o/\cos\alpha)}{\sin^2\alpha}\right]^{-1} \qquad (2.26)$$

Expanding the integrand in Eq. (2.25) and maintaining only the first-order term in X gives

$$s_2 = \frac{f}{c} r_o \int_o^{\pi/2} \frac{X(r_o/\cos\alpha)}{\cos^2\alpha} d\alpha \qquad (2.27)$$

which is the same as integrating X along a straight line through the ionosphere. It is important to notice here that while refraction can be neglected as far as computation of s_2 goes, one cannot at all neglect the influence of refraction on s_p or s_g when the receiver is well behind the ionosphere.

Combining Eq. (2.15) and Eq. (2.27), one obtains:

$$2\psi = -\frac{c}{f} \frac{ds_2(r_o)}{dr_o} \qquad (2.28)$$

which will prove useful in later chapters.

The time rate of change in s_p gives the doppler shift due to the ionosphere. One may measure ds_p/dt in the following way. Assume that two harmonically related frequencies f_1 and f_2 are transmitted from the earth. Thus $f_1 m = f_2$, where m is an integer larger than 1. Before occultation takes place, one will receive the frequencies $f_1[1 - (v_r/c)]$ and $f_2[1 - (v_r/c)]$, where v_r is the velocity at which the transmitter and receiver move apart. The lowest frequency will in addition be shifted by Δf_i during occultation. We will assume that f_2 is so high that this wave propagates undisturbed through the planetary ionosphere. After mixing of $f_2[1 - (v_r/c)]$ and the m^{th} harmonic of $f_1[1 - (v_r/c)] - \Delta f_i$, one can filter out $m\Delta f_i$. This yields s_p after integration. It is here assumed that the effect of

changes in the earth's ionosphere and in the interplanetary medium can be neglected or predicted.

The total electron content of the earth's ionosphere is about $2 \cdot 10^{17}$ electrons/meter^2 in the daytime. Ionospheric irregularities cause fluctuations of about ±2 percent in the daytime content [Ref. 4]. This variation corresponds to a change in s_2 of about ±10 wavelengths at frequency 50 Mc. Nighttime variations in s_2 would be smaller.

Even less is known about the density fluctuations one may encounter in the interplanetary medium. However, the Stanford Center for Radar Astronomy has radio propagation experiments to be included on Pioneer I and II which will help answer these questions.

Group-path measurements may also be used. This can be done by transmitting two pulse trains of frequency f_1 and f_2, respectively, and observing the change in the time delay between pulses of different frequency.

Other possible measurement techniques are discussed by Eshleman, Gallagher, and Barthle [Ref. 5].

C. REFRACTION GAIN (G_r)

Another measurable quantity of great interest is the amplitude of the signal. Rather than compute the absolute value of the amplitude, we will find the changes in the amplitude due to the presence of the planetary ionosphere.

Let us define the "refraction gain" (G_r) as

$$G_r = 10 \log \frac{S_2}{S_1} \qquad \text{(db)} \tag{2.29}$$

where S_1 is the Poynting vector one would have at the position of the receiver without any planetary ionosphere, and S_2 is the Poynting vector at the receiver in the presence of the ionosphere. Figure 8 illustrates, considerably exaggerated, the effect of refraction on the amplitude. We will assume that the gain of the transmitting antenna can be considered constant over a solid angle, including that part of the fly-by trajectory along which the occultation is observed. This assumption implies that, in the absence of any planetary ionosphere, the power

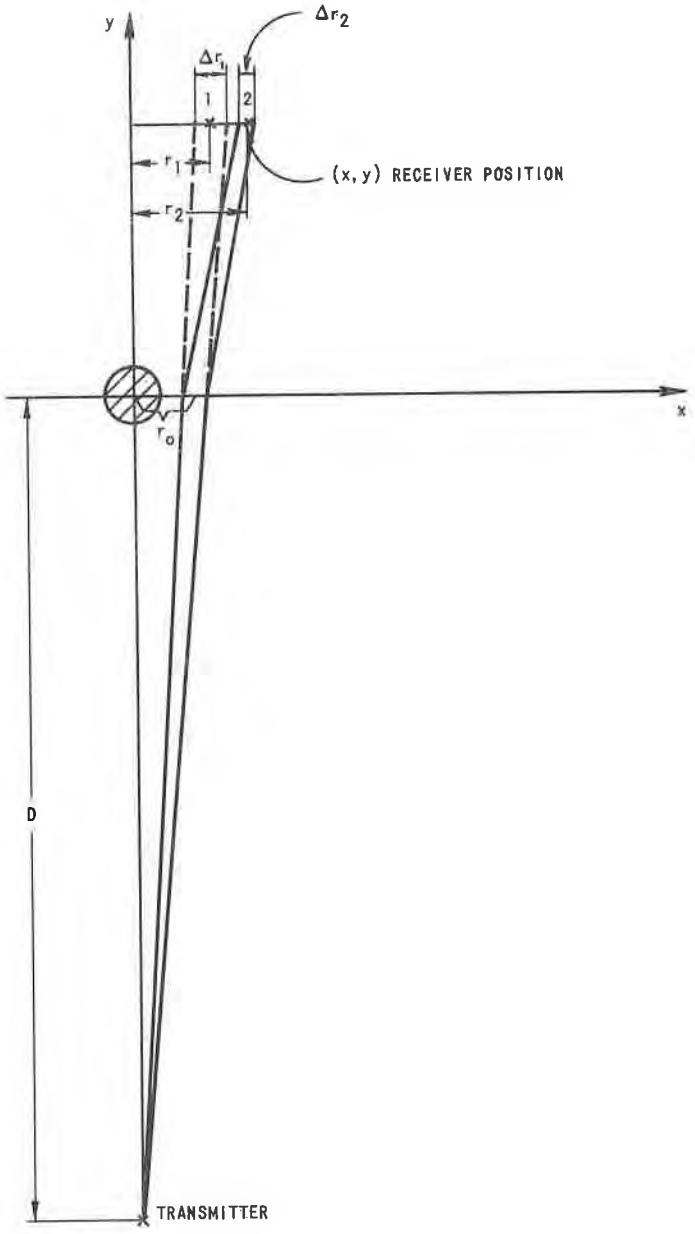

FIG. 8. REFRACTION GAIN DUE TO PLANETARY ATMOSPHERE.

density is the same at positions 1 and 2 in Fig. 8. Hence one can relate S_1 and S_2 to geometric quantities on the ray picture

$$S_1 r_1 \Delta r_1 = S_2 r_2 \Delta r_2$$

which gives

$$G_r = 10 \log \left(\frac{r_1 \Delta r_1}{r_2 \Delta r_2} \right) \tag{2.30}$$

We can simplify Eq. (2.30) further because the angle by which the rays are refracted (2ψ) is very small in the high-frequency case. Let the coordinates of the receiver be (x,y). We have, using quantities defined in Fig. 5:

$$r_2 = R_P + q + (2\psi + \beta) y$$

and

$$r_1 = \frac{a}{\cos \beta} + \beta y$$

After introducing $r_2 = x$, one obtains

$$\frac{r_1}{r_2} \approx 1 - 2\psi \frac{y}{x} \tag{2.31}$$

where only first-order terms in 2ψ and β are maintained. We can also write

$$\Delta r_2 = \Delta r_1 + \frac{d2\psi}{dr_o} \Delta r_1 \frac{Dy}{D + y} \tag{2.32}$$

Combining Eqs. (2.30), (2.31), and (2.32), one obtains

$$G_r = 10 \log \left| \frac{1 - 2\psi \frac{y}{x}}{1 + \frac{d2\psi}{dr_o} \frac{Dy}{D + y}} \right| \tag{2.33}$$

Close behind the ionosphere one has

$$\left| 2\psi \frac{y}{x} \right| \ll 1$$

$$\left| \frac{d2\psi}{dr_o} \frac{Dy}{D + y} \right| \ll 1$$

and this gives for the gain

$$G_r \approx 4.34 \left(- \frac{d2\psi}{dr_o} y - 2\psi \frac{y}{x} \right) \qquad (2.34)$$

where one can often neglect the term $(2\psi\, y/x)$.

We have here based the definition of the gain on the ray theory. This implies that G_r does not describe the amplitude variations close to shadow boundaries or caustics. Approximations for the amplitude can in these regions be found from the wave theory as shown in Appendix A.

D. CAUSTIC FORMATION

The distance (y_c) behind the ionosphere at which the rays cross each other can be found by setting the denominator of Eq. (2.33) equal to zero:

$$1 + \frac{d2\psi}{dr_o} \frac{Dy_c}{D + y_c} = 0$$

or

$$y_c = \left(- \frac{d2\psi}{dr_o} - \frac{1}{D} \right)^{-1} \qquad (2.35)$$

Caustics are formed only when

$$\frac{d2\psi}{dr_o} < - \frac{1}{D} \qquad (2.36)$$

for some finite interval in r_o, while $d2\psi/dr_o > - 1/D$ tends to defocus the energy.

III. APPLICATION TO AN IONOSPHERE WITH EXPONENTIAL ELECTRON DENSITY DISTRIBUTION

One can, for planetary atmospheres in hydrostatic equilibrium, show that the electron density will be an exponential function of height when the density in the atmosphere is sufficiently low. This is a special case of the Chapman theory [Ref. 6].

We will in this chapter use

$$X(r) = X_s \exp\left(-\frac{r - R_p}{2H}\right) \tag{3.1}$$

where X_s is the normalized electron density at the surface, H is the scale height in the atmosphere, and R_p is the planetary radius.

The complete Chapman formula will be used in the next chapter.

A. RAYPATHS

The raypaths can be determined by combining Eq. (2.6) and Eq. (3.1). However, it is sufficient for our purpose to know the raypath asymptotes and these are determined by Eqs. (2.8) and (2.12). Using Eqs. (2.12) and (3.1), we obtain the angle of refraction (2ψ):

$$\frac{2\psi}{X(r_o)} = \int_o^{\pi/2} \frac{1 - \exp\left[\frac{r_o}{2H}\left(1 - \frac{1}{\cos\alpha}\right)\right]}{\sin^2\alpha}\, d\alpha \tag{3.2}$$

This is shown in Fig. 9 as a function of $r_o/2H$.

Equation (3.2) gives the high-frequency approximation for 2ψ. However, we would also like to know what accuracy we can expect from the high-frequency approximation. This can be seen by comparing it with the exact solution. Combining Eq. (2.10) and Eq. (3.1), we find the exact solution:

$$\frac{2\psi}{X(r_o)} = \frac{2}{X(r_o)} \int_o^{\pi/2} 1 - \left\{ \frac{1 - X(r_o)}{1 + X(r_o)\,\dfrac{\cos^2\alpha - \exp\left[-\frac{r_o}{2H}\left(1 - \frac{1}{\cos\alpha}\right)\right]}{\sin^2\alpha}} \right\}^{1/2} d\alpha \tag{3.3}$$

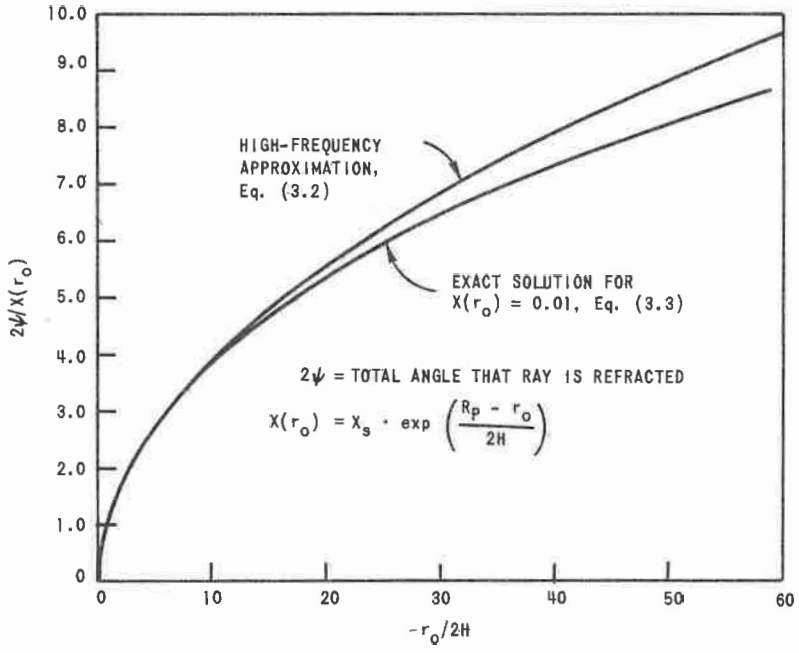

FIG. 9. NORMALIZED ANGLE OF REFRACTION FOR THE EXPONENTIAL IONOSPHERE.

The right-hand side is in this case a function both of $r_o/2H$ and $X(r_o)$. It is therefore necessary to choose some particular value of $X(r_o)$ in order to compare the two solutions given by Eq. (3.2) and Eq. (3.3) respectively. With $X(r_o) = 0.01$ in Eq. (3.3) one obtains the lower curve in Fig. 9.

Figure 9 may give the false impression that the accuracy in 2ψ is decreasing with increasing r_o when the high-frequency approximation is used. However, this is not true because $X(r_o)$ falls off very fast with increasing r_o.

As an example, let us use $H = 50$ km and $X_s = 0.01$ for the moon. This gives $r_o/2H \approx 17$ for the grazing ray. From Fig. 9 we find that this corresponds to an error in 2ψ of about 3 percent. The error is less for rays missing the surface.

It may seem surprising that the curves on Fig. 9 go through the origin. This may occur in two different situations:

1. In the $r_o = 0$ case, there is no planet in the center of the ionosphere. The ray passing through the center of the ionized blob is not bent in any direction.
2. In the $1/H = 0$ case, 2ψ is also zero because there is no gradient in the ionization.

The curves in Fig. 9 have been found by integrating Eq. (3.2) and Eq. (3.3) on a digital computer. Analytic techniques can also be employed. One can, for instance, expand the integrand into the following form:

$$\exp(-k\alpha^2) \sum_{\nu = 0,4,6,\ldots} c_\nu \alpha^\nu \tag{3.4}$$

This form enables us to evaluate the integral when the upper limit $(\pi/2)$ can be replaced by infinity. For 2ψ one can derive

$$2\psi \approx \frac{1}{2} X_s \left(\frac{\pi r_o}{H}\right)^{1/2} \exp\left(\frac{R_p - r_o}{2H}\right) \left[1 - \frac{3}{16} \frac{r_o}{2H} X(r_o)\right] \tag{3.5}$$

A numeric example has been worked out in order to illustrate the theory developed so far. The example assumes an exponential model for the lunar ionosphere with $R_p = 1738$ km, $H = 50$ km, $f = 50$ Mc, and an electron density at the surface equal to 200 electrons/cm^3 ($X_s = 6.44 \cdot 10^{-6}$). The corresponding ray picture is shown in Fig. 10. The scale is different along the two axes, and the moon will therefore look like an ellipsoid in this space. The waves are assumed to be transmitted from the earth.

B. PHASE PATH (s_p) AND GROUP PATH (s_g)

It was shown in Sec. IIB that the changes in the group path and the phase path, due to the planetary ionosphere, can conveniently be expressed as the sum of, and the difference between, s_2 and s_1,

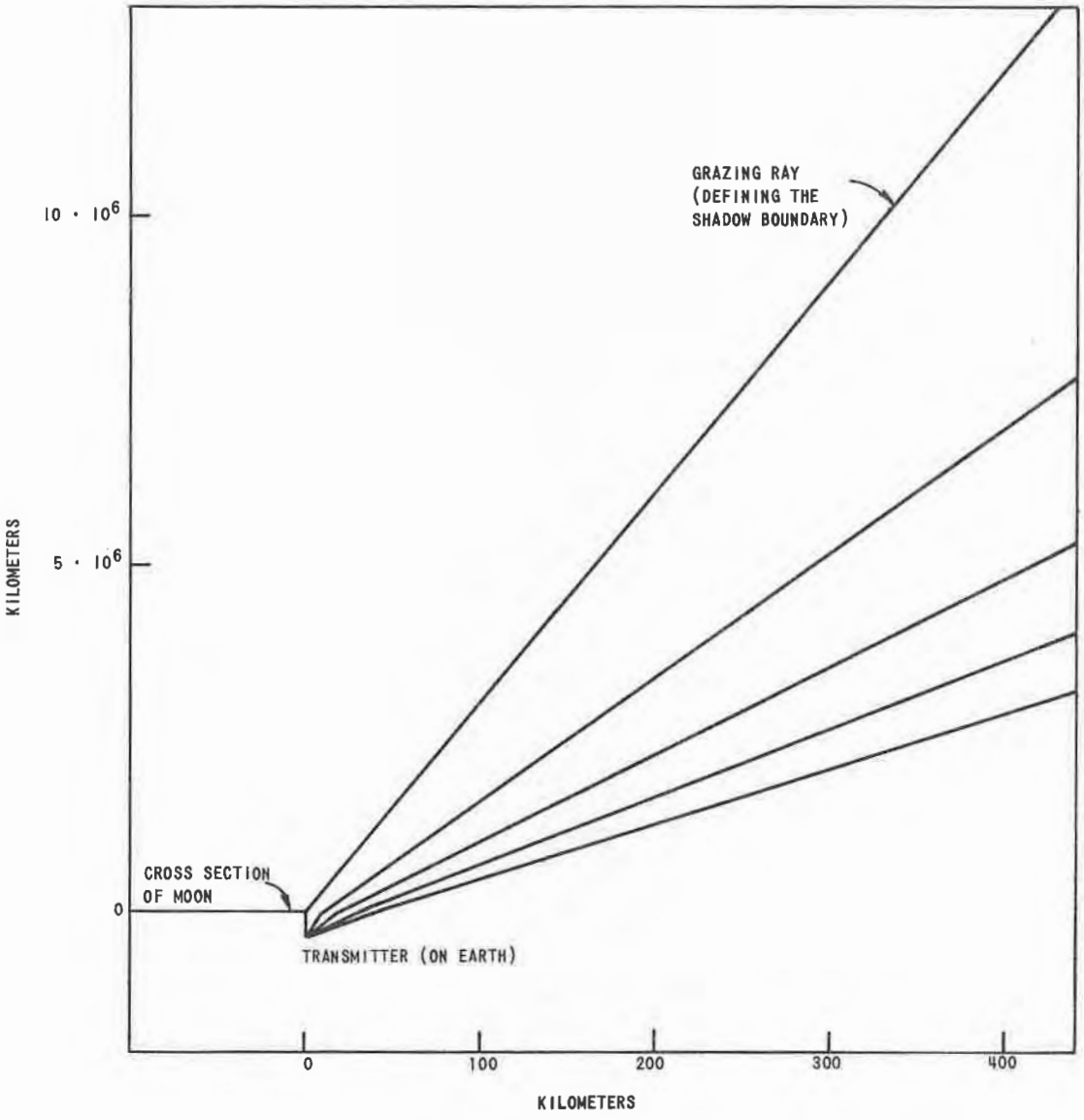

FIG. 10. REFRACTION IN A LUNAR IONOSPHERE AT 50 Mc WITH THE TRANSMITTER ON THE EARTH. (Assumed electron density: $N(h) = N_{max} \exp(-h/2H)$, where $N_{max} = 2 \cdot 10^8$ electrons/m^3; H = 50 km.)

respectively. Here s_2 is approximately proportional to the electron density integrated along straight lines, and s_1 is proportional to the difference in path length with and without the planetary ionosphere.

The high-frequency approximation for s_2 is given by Eq. (2.27). Combining this with Eq. (3.1), one obtains:

$$\frac{cs_2}{fr_o X(r_o)} = \int_o^{\pi/2} \frac{\exp\left[\frac{r_o}{2H}\left(1 - \frac{1}{\cos\alpha}\right)\right]}{\cos^2\alpha}\, d\alpha \qquad (3.6)$$

The result is shown in Fig. 11 as a function of $r_o/2H$ (upper curve).

Equation (3.6) gives the high-frequency approximation for s_2. We also like to know what accuracy we can expect from the high-frequency approximation. One can determine the accuracy of Eq. (3.6) by comparing it with the exact solution given by Eq. (2.25) and Eq. (2.26). The exact solution can be normalized in the same way as Eq. (3.6). However, the right-hand side will be a function both of $r_o/2H$ and $X(r_o)$. It

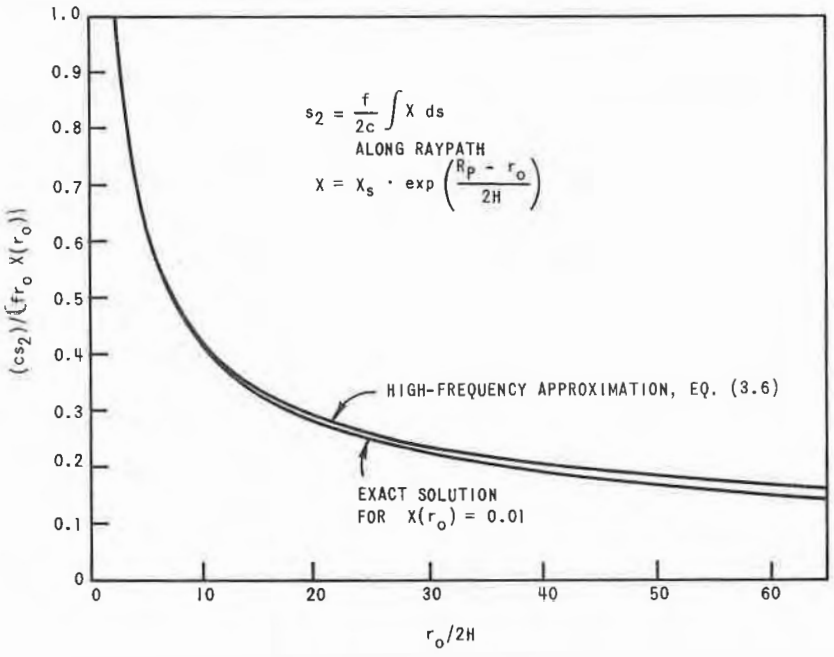

FIG. 11. NORMALIZED s_2 FOR THE EXPONENTIAL IONOSPHERE.

is therefore necessary to keep $X(r_o)$ constant in order to compare the exact solution with the high-frequency approximation. Choosing $X(r_o) = 0.01$, one finds the lower curve in Fig. 11.

The pole at the origin in Fig. 11 is caused by the normalization and does not mean that s_2 is infinite for a ray passing through the center of a blob of exponentially distributed ionization.

The curves on Fig. 11 have been obtained by evaluating the integrals on a computer. Analytic techniques can also be employed, as already mentioned in Sec. IIIA. For instance, one can show that:

$$s_2 \approx \frac{f}{c} \sqrt{\pi H r_o}\, X(r_o) \tag{3.7}$$

For certain intervals in $r_o/2H$, one can find better approximations for s_2.

We also need to find s_1 given by Eq. (2.21). The rays can first be replaced by their asymptotes as described in Sec. IIB. This computation does not require any new integration when ψ is known. Equation (2.24) gives s_1 when the waves can be considered plane before they are refracted in the planetary ionosphere. The term Δs_1 is the difference between the phase path measured along the raypath and the phase path measured along the raypath asymptotes.

The term Δs_1 can be approximated in different ways. For instance, one can replace that part of the raypath that is closest to the planetary ionosphere by an arc of a circle. This raypath shape gives

$$\Delta s_1 = 2 \frac{f}{c} (\psi - \tan \psi)\, r_o \left(1 - \frac{a}{r_o} \sec \psi\right) \frac{1}{\sec \psi - 1} \approx - \frac{2}{3} \frac{f}{c}\, r_o \psi X(r_o) \tag{3.8}$$

which is usually negligible at high frequencies.

The raypath is not really an arc of a circle close to the surface, and it is therefore necessary to check how much the actual shape of the raypath will influence the form of the expression for Δs_1. For instance, one can replace the arc of the circle by a piece of a parabola with maximum curvature at the point of closest approach. (The reason for choosing a parabola is, of course, that the line integral of this conic section can be found in terms of elementary functions.) By comparing the two results one finds that the difference in Δs_1 is negligible.

The reason why s_1 can be approximated in such a simple way is, of course, that the raypaths are almost straight lines.

C. REFRACTION GAIN (G_r)

The refraction gain (G_r) was defined in Sec. IIC as the change in signal strength due to the refraction in the planetary ionosphere. Equation (2.33) shows that this gain depends on which part of the ionosphere the signal is propagating through and how far the receiver is behind the planetary ionosphere. The numerator of Eq. (2.33) contains 2ψ which can be found from Eq. (3.5), and the denominator of Eq. (2.33) can be approximated in the following way:

$$1 + \frac{d(2\psi)}{dr_o}\frac{Dy}{D+y} \approx 1 - \frac{Dy}{D+y}\frac{X_s}{2}\left(\frac{\pi R_p}{H}\right)^{1/2} \exp\left(\frac{R_p - r_o}{2H}\right)\left[\frac{1}{2H} - \frac{1}{2R_p} + \frac{r_o - R_p}{4HR_p}\right] \tag{3.9}$$

where 2ψ has been approximated by

$$2\psi \approx \frac{X_s}{2}\left(\frac{\pi R_p}{H}\right)^{1/2}\left[1 + \frac{1}{2}\frac{r_o - R_p}{R_p}\right]\exp\left(\frac{R_p - r_o}{2H}\right)$$

D. CAUSTIC FORMATION

An approximation for the caustic can be found by combining Eq. (2.35) and Eq. (3.5). This corresponds to setting the right-hand side of Eq. (3.9) equal to zero. One then obtains for the y-coordinate (y_c) of the caustic:

$$y_c \approx \left[-\frac{1}{D} + \frac{X_s}{2}\left(\frac{\pi R_p}{H}\right)^{1/2}\left(\frac{1}{2H} - \frac{1}{2R_p} + \frac{r_o - R_p}{4R_p H}\right)\exp\left(\frac{R_p - r_o}{2H}\right)\right]^{-1} \tag{3.10}$$

This expression can be simplified further when $H \ll R_p$ and $r_o - R_p \ll 2R_p$. If one also approximates x_c with $(r_o + y_c 2\psi)$, one obtains

$$\frac{x_c - R_p}{2H} \approx 1 + \frac{y_c}{D} - \ln\left[\frac{4H}{X_s}\left(\frac{H}{\pi R_p}\right)^{1/2}\left(\frac{1}{D} + \frac{1}{y_c}\right)\right] \tag{3.11}$$

where (x_c, y_c) designates the coordinates of the caustic.

A ray picture was shown in Fig. 10, but it did not have any caustic, the reason being that the curvature of the wavefronts was too large before the waves were refracted in the lunar ionosphere. However, the result will look different if the wavefronts are assumed plane before they are refracted in the moon's ionosphere. This is illustrated in Fig. 12. The ionospheric model and the frequency are the same as in the previous example shown in Fig. 10, but the source is at infinity.

The caustic in Fig. 12 is given by Eq. (3.11) with $1/D = 0$, which gives

$$y_c \approx \frac{4H}{X_s} \left(\frac{H}{\pi R_p} \right)^{1/2} \exp \left(-1 + \frac{x_c - R_p}{2H} \right) \tag{3.12}$$

In order to have a caustic, it is necessary that y_c in Eq. (3.10) be positive for some finite interval in r_o. This requires that

$$X_s > \frac{4}{D} \left(\frac{H}{\pi R_p} \right)^{1/2} \left(\frac{1}{H} - \frac{1}{R_p} \right)^{-1} \tag{3.13}$$

We note that at sufficiently low frequencies there will exist a caustic, but as the frequency is increased, X_s ceases to satisfy the above relation, and the caustic disappears.

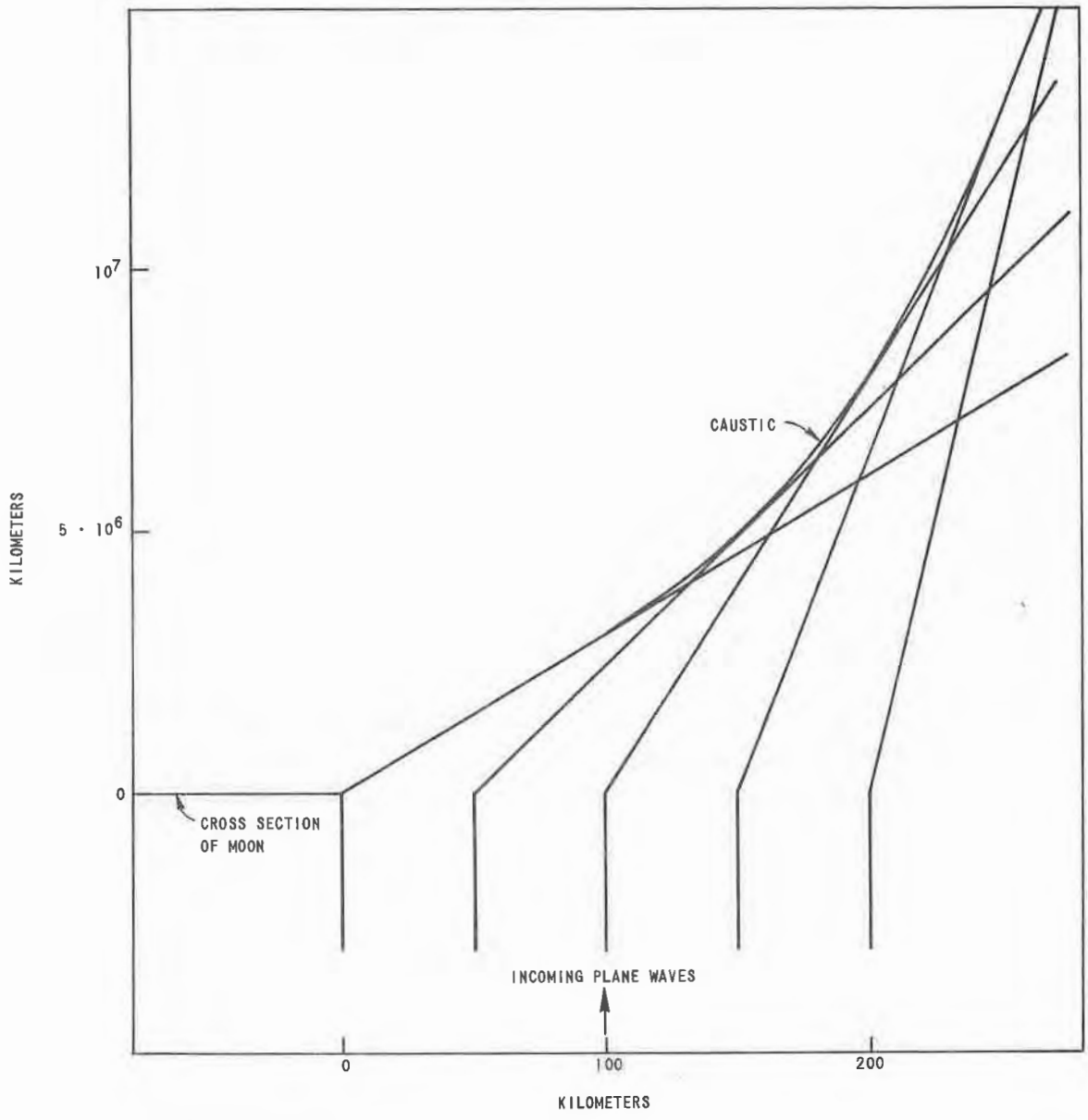

FIG. 12. REFRACTION IN A LUNAR IONOSPHERE AT 50 Mc WITH THE SOURCE AT INFINITY. (Assumed electron density: $N(h) = N_{max} \exp(-h/2H)$, where $N_{max} = 2 \cdot 10^8$ electrons/m^3; H = 50 km.)

IV. APPLICATION TO AN IONOSPHERE WITH CHAPMAN-DISTRIBUTED ELECTRON DENSITY

The Chapman theory [Ref. 6] gives the electron density as a function of solar zenith angle (χ) and radial distance from the center of the planet (r). Normalizing the Chapman electron density distribution using Eq. (2.5), one obtains:

$$X\left(\frac{r_o}{\cos\alpha},\chi\right) = X_{max}\ \exp\left\{\frac{1}{2}\left[1 + \frac{R_p+h_o}{H} - \frac{r_o}{H\cos\alpha} - \sec\chi\ \exp\left(\frac{R_p+h_o}{H} - \frac{r_o}{H\cos\alpha}\right)\right]\right\} \tag{4.1}$$

where $r_o/\cos\alpha$ represents the distance to the center of the planet (r) [using Eq. (2.9)], χ is the solar zenith angle, H is the scale height in the atmosphere, R_p is the radius of the planet, h_o is the height of the maximum electron density at $\chi = 0$, and X_{max} is the maximum in the normalized electron density. The Chapman ionosphere is not spherically symmetric.

The signal transmitted from the earth and received in a space probe behind the Chapman ionosphere will only propagate through part of the planetary ionosphere. The variations in the electron density with longitude and latitude can be neglected as a first approximation in that part of the ionosphere which is probed by the waves. This corresponds to setting χ in Eq. (4.1) equal to a constant χ_o. For χ_o we will use the solar zenith angle at the point where the ray passing through the receiver is closest to the planet.

Equation (4.1) can now be rewritten in a more convenient form:

$$X\left(\frac{r_o}{\cos\alpha}\right) = X_{max}\sqrt{\cos\chi_o}\ \exp\left\{\frac{1}{2}\left[1 + K - \frac{r_o}{H\cos\alpha} - \exp\left(K - \frac{r_o}{H\cos\alpha}\right)\right]\right\} \tag{4.2}$$

where

$$K = \frac{R_p + h_o}{H} + \ln\sec\chi_o \tag{4.3}$$

Equation (4.2) represents the normalized electron density distribution in a spherically symmetric ionosphere. The maximum X is

$X_{max}\sqrt{\cos \chi_o}$ at a height h_{max}. The height h_{max} is given by

$$h_{max} = h_o + H \ln \sec \chi_o \tag{4.4}$$

It is important to notice here that we are not replacing the entire Chapman ionosphere with a spherically symmetric ionosphere. We are merely neglecting the nonspherical variations in the relatively small part of the ionosphere which is probed by the signal. This simplification will be further justified later.

A. RAYPATHS

Section IIA describes how one can determine the raypath asymptotes when the ionosphere is given. The determination of the raypath asymptotes mainly amounts to calculation of the angle (2ψ) that the rays are refracted.

Combining Eqs. (2.12) and (4.2), one obtains the high-frequency approximation for 2ψ:

$$\frac{2\psi}{X_{max}}\sqrt{\sec \chi_o} = \int_o^{\pi/2} \left(\frac{\exp\left\{\frac{1}{2}\left[1 + K - \frac{r_o}{H} - \exp\left(K - \frac{r_o}{H}\right)\right]\right\}}{\sin^2\alpha} - \frac{\exp\left\{\frac{1}{2}\left[1 + K - \frac{r_o}{H\cos\alpha} - \exp\left(K - \frac{r_o}{H\cos\alpha}\right)\right]\right\}}{\sin^2\alpha} \right) d\alpha \tag{4.5}$$

The right-hand side can be considered a function of K and $(h-h_{max})/2H$. Here h denotes the height at which the ray is missing the surface, thus h is equal to $(r_o - R_p)$. The result of integrating Eq. (4.5) is shown in Fig. 13.

Figure 14 gives an indication of what accuracy one can expect from the high-frequency approximation by comparing it with the exact solution. The exact solution is found by combining Eq. (2.10) and Eq. (4.2). Normalizing the exact solution in the same way as in Eq. (4.5), one obtains a function of K, $(h-h_{max})/2H$, and $X_{max}\sqrt{\cos \chi_o}$ on the right-hand side of the equal sign. The curve representing the exact solution in Fig. 14 is drawn for $K = 30$ and $X_{max}\sqrt{\cos \chi_o} = 0.01$.

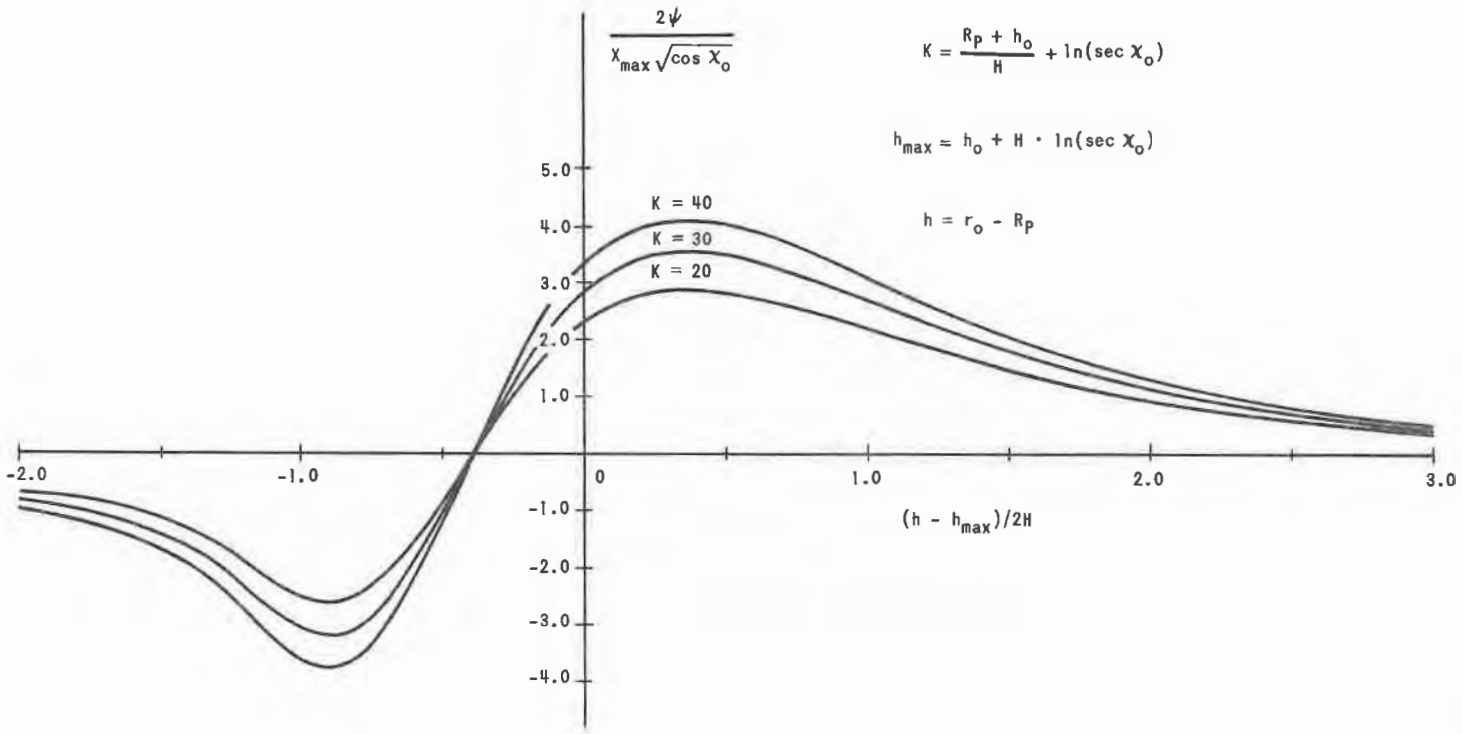

FIG. 13. NORMALIZED ANGLE OF REFRACTION FOR THE CHAPMAN IONOSPHERE.

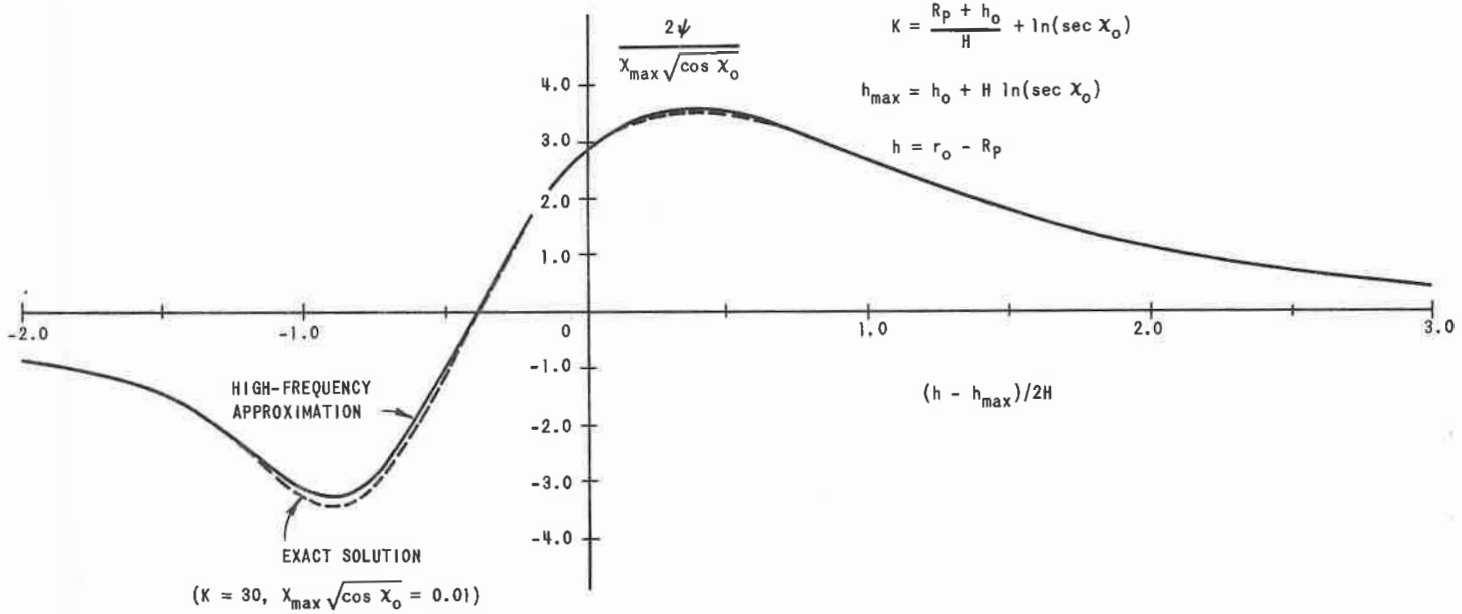

FIG. 14. COMPARISON BETWEEN EXACT AND APPROXIMATE REFRACTION ANGLE FOR THE CHAPMAN IONOSPHERE.

B. PHASE PATH (s_p) AND GROUP PATH (s_g)

It was shown in Sec. IIB how the changes in group path or phase path, due to the planetary ionosphere, can be expressed respectively as the sum of or the difference between s_1 and s_2.

Sections IIB and IIIB showed that s_1 can be approximated as the phase path along the raypath asymptotes minus the phase path along a straight line connecting transmitter and receiver. Thus s_1 can be found without integration when the raypath asymptotes are determined.

Equation (2.27) gives the high-frequency approximation for s_2. Combining Eq. (2.27) and Eq. (4.2), one obtains:

$$\frac{cs_2}{fX_{max}r_o}\sqrt{\sec\chi_o} = \int_o^{\pi/2} \exp\left\{\frac{1}{2}\left[1 + K - \frac{r_o}{H\cos\alpha} - \exp\left(K - \frac{r_o}{H\cos\alpha}\right)\right]\right\}\frac{d\alpha}{\cos^2\alpha} \tag{4.6}$$

The result is shown in Fig. 15 where h is the raypath miss distance and h_{max} is the height of the maximum electron density.

Figure 16 shows a comparison between the high-frequency approximation given by Eq. (4.6) and the exact solution given by Eqs. (2.25), (2.26), and (4.2) for $K = 30$ and $X_{max}\sqrt{\cos\chi_o} = 0.01$.

For large values of $(h-h_{max})/2H$, one can use the results in Chapter III.

The integrals in this chapter have mainly been evaluated on a digital computer, but analytic techniques can also be employed. The integrand in Eq. (4.6) can for instance be expanded as described in Chapter III. However, different intervals in α require different expansions, and it is therefore difficult to obtain good accuracy when adding and subtracting the different areas. For rays that do not pass inside the maximum in the electron density, one can show that

$$s_2 \approx \frac{f}{c}X_{max}(\pi H r_o\cos\chi_o)^{1/2}\exp\left[\frac{1}{2}\left(1 + K - \frac{r_o}{H}\right)\right]\left\{\frac{3}{8} + \frac{2}{3}\exp\left[-\frac{1}{2}\exp\left(K - \frac{r_o}{H}\right)\right]\right\} \tag{4.7}$$

Similar approximations have been found for other intervals in $(h-h_{max})/2H$, but the accuracy of these approximations is not very good and they are therefore not given here.

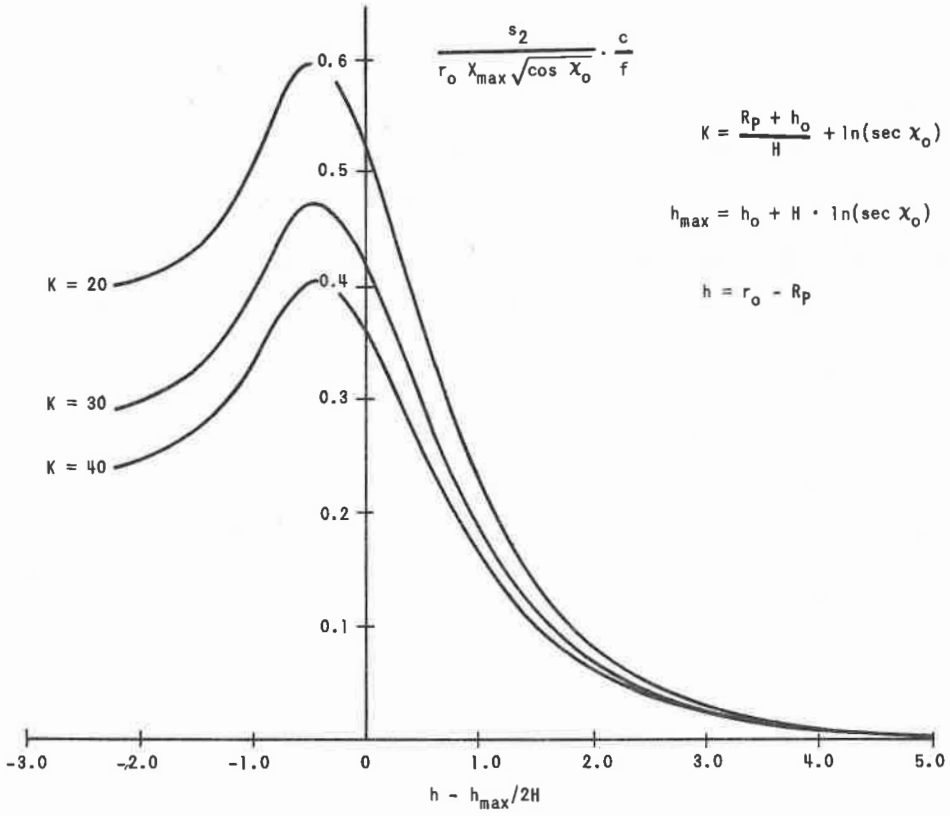

FIG. 15. NORMALIZED s_2 FOR THE CHAPMAN IONOSPHERE.

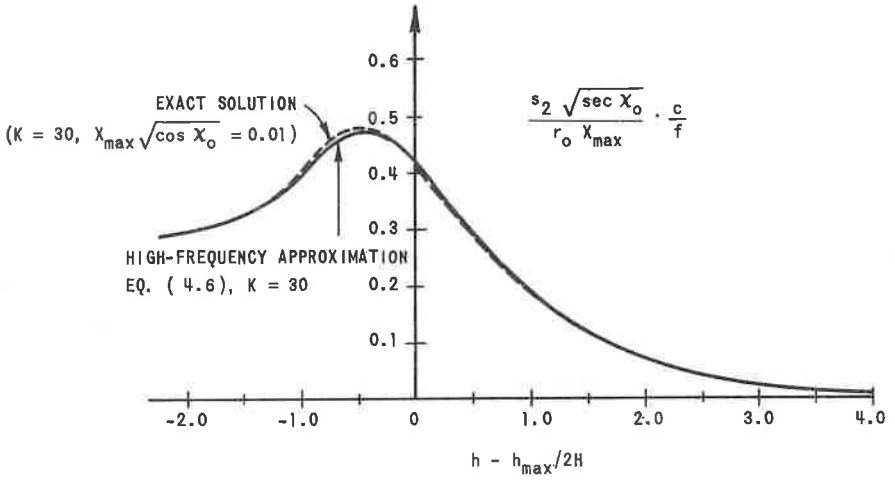

FIG. 16. COMPARISON BETWEEN EXACT AND APPROXIMATE s_2 FOR THE CHAPMAN IONOSPHERE.

C. CAUSTICS

The refraction gain (G_r) behind a Chapman ionosphere can be computed using Sec. IIC and Sec. IVA. The gain G_r is infinite along caustics and this fact is made use of in Sec. IID to obtain the equation for the caustic [Eq. (2.35)].

Combining Eq. (4.5) and Eq. (2.35), one obtains for the caustic ordinate y_c behind a Chapman ionosphere:

$$\frac{y_c}{1+\frac{y_c}{D}}\ \frac{X_{max}}{2H}\sqrt{\cos\chi_o} = \left[-\int_0^{\pi/2}\frac{d}{d\left(\frac{r_o}{2H}\right)}\left(\exp\left|\frac{1}{2}\left[1+K-\frac{r_o}{H}-\exp\left(K-\frac{r_o}{H}\right)\right]\right|\right.\right.$$

$$\left.\left.-\exp\left|\frac{1}{2}\left[1+K-\frac{r_o}{H\cos\alpha}-\exp\left(K-\frac{r_o}{H\cos\alpha}\right)\right]\right|\right)\frac{d\alpha}{\sin^2\alpha}\right]^{-1} \tag{4.8}$$

The result is shown in Fig. 17 as a function of $(h-h_{max})/2H$, where h is the raypath miss distance and h_{max} is the height at which the electron density has its maximum. We see from Fig. 17 that two caustics may exist behind a Chapman ionosphere.

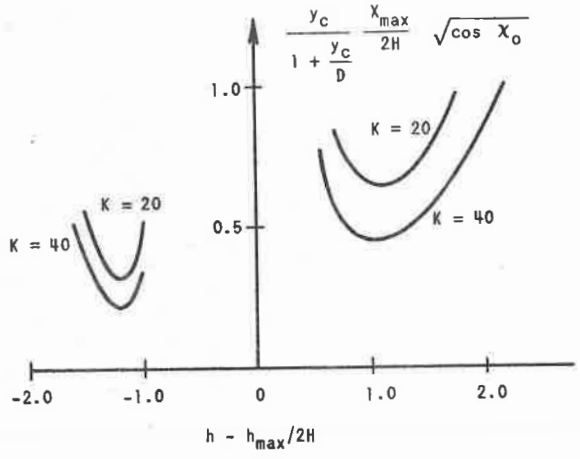

FIG. 17. NORMALIZED DISTANCE TO THE CAUSTIC FOR THE CHAPMAN IONOSPHERE.

D. NUMERIC EXAMPLE USING A CHAPMAN MODEL FOR THE MARTIAN IONOSPHERE

The previous sections have shown how the refractive properties of the Chapman layer can be represented graphically in a normalized form. In this section a numeric example is given assuming that Mars has a Chapman ionosphere. The signals are transmitted from the earth and received in a spacecraft that is being occulted by the Martian ionosphere. We will compute phase path and refraction gain of the signal received in the spacecraft. The geometry is illustrated in Fig. 18. Two receiver trajectories are shown.

The radial distribution of the electron density along the x axis is shown in Fig. 19. We will first neglect the nonspherical variations in the electron density distribution, thus

$$\chi = \chi_o$$

where χ_o is the angle between the x axis and the direction to the sun. This approximation will be justified later.

Figure 20 shows the ray picture in the x-y plane for $f = 50$ Mc. The curvature of the wavefront is much smaller before it reaches Mars than after it has been refracted in the Martian ionosphere. The waves have therefore, for simplicity, been assumed plane before they are refracted in the Martian ionosphere.

The atmosphere on Mars also causes refraction. Chapter III, with X defined by Eq. (2.18), is well suited for making estimates of the atmospheric effects. Reference 7 gives the necessary atmospheric parameters for Mars. Using these parameters one finds that the effect of the atmosphere can be neglected.

Figures 21 and 22 show how amplitude and phase change when occultation takes place along trajectory 1. The doppler shift of the signal, caused by the Martian ionosphere, is given by

$$+\frac{ds_p}{dt} = \frac{ds_p}{dx}\left(\frac{+dx}{dt}\right) \qquad \text{cps}$$

The first factor (ds_p/dx) is shown as a function of receiver miss distance $(x - R_p)$ in Fig. 23. For $-dx/dt = 10^3$ m/sec we see that

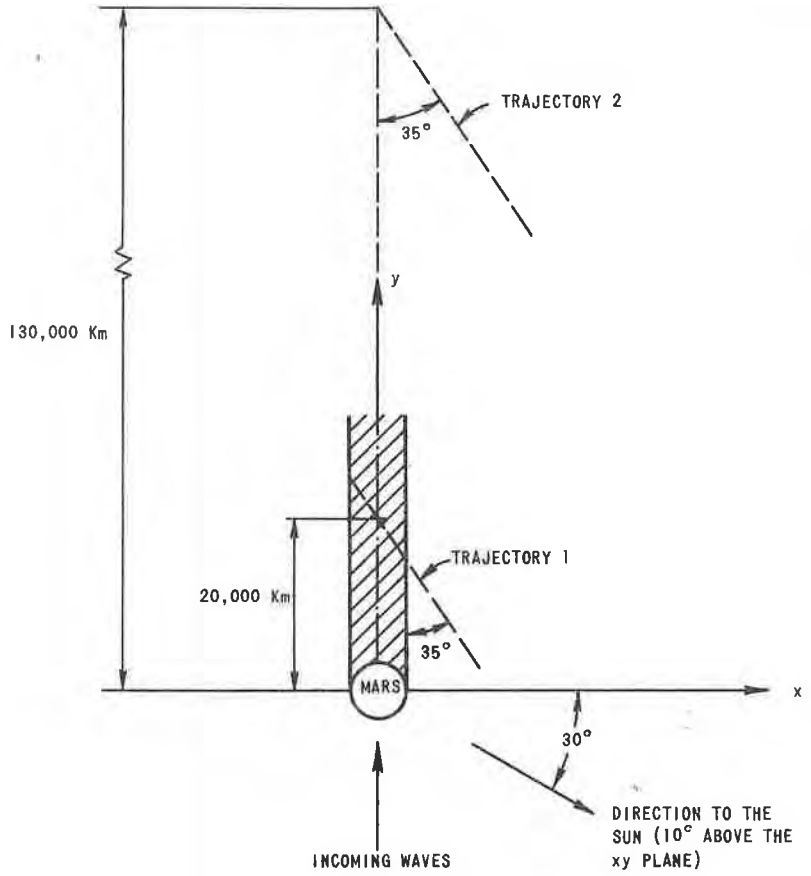

FIG. 18. ASSUMED GEOMETRY DURING OCCULTATION.

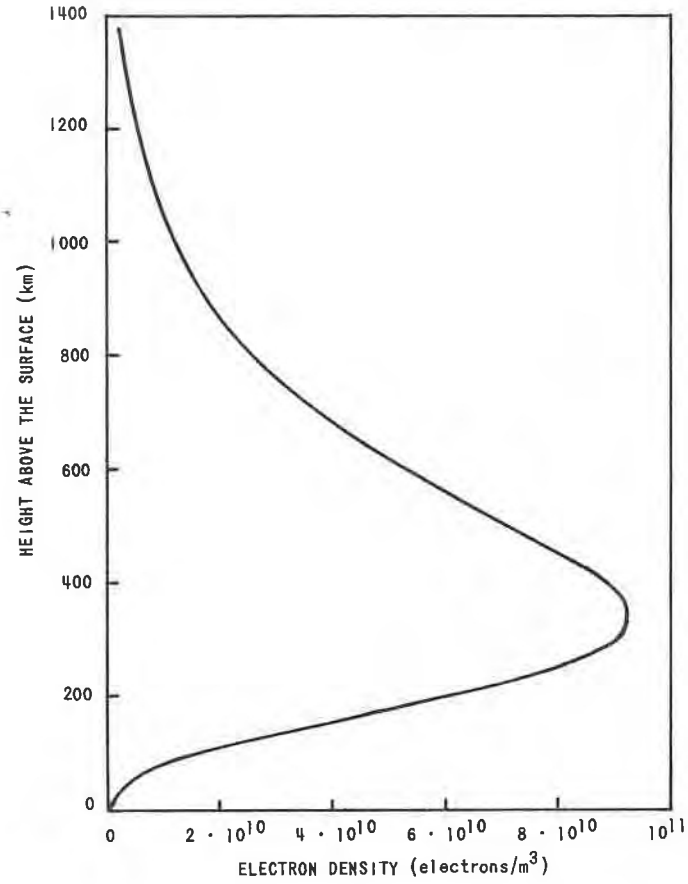

FIG. 19. ASSUMED ELECTRON DENSITY PROFILE. (Chapman layer, $H = 130$ km, $h_o = 320$ km, $N_{max} = 10^{11}$ electrons/m^3, $\sec \chi_o = 1.175$.)

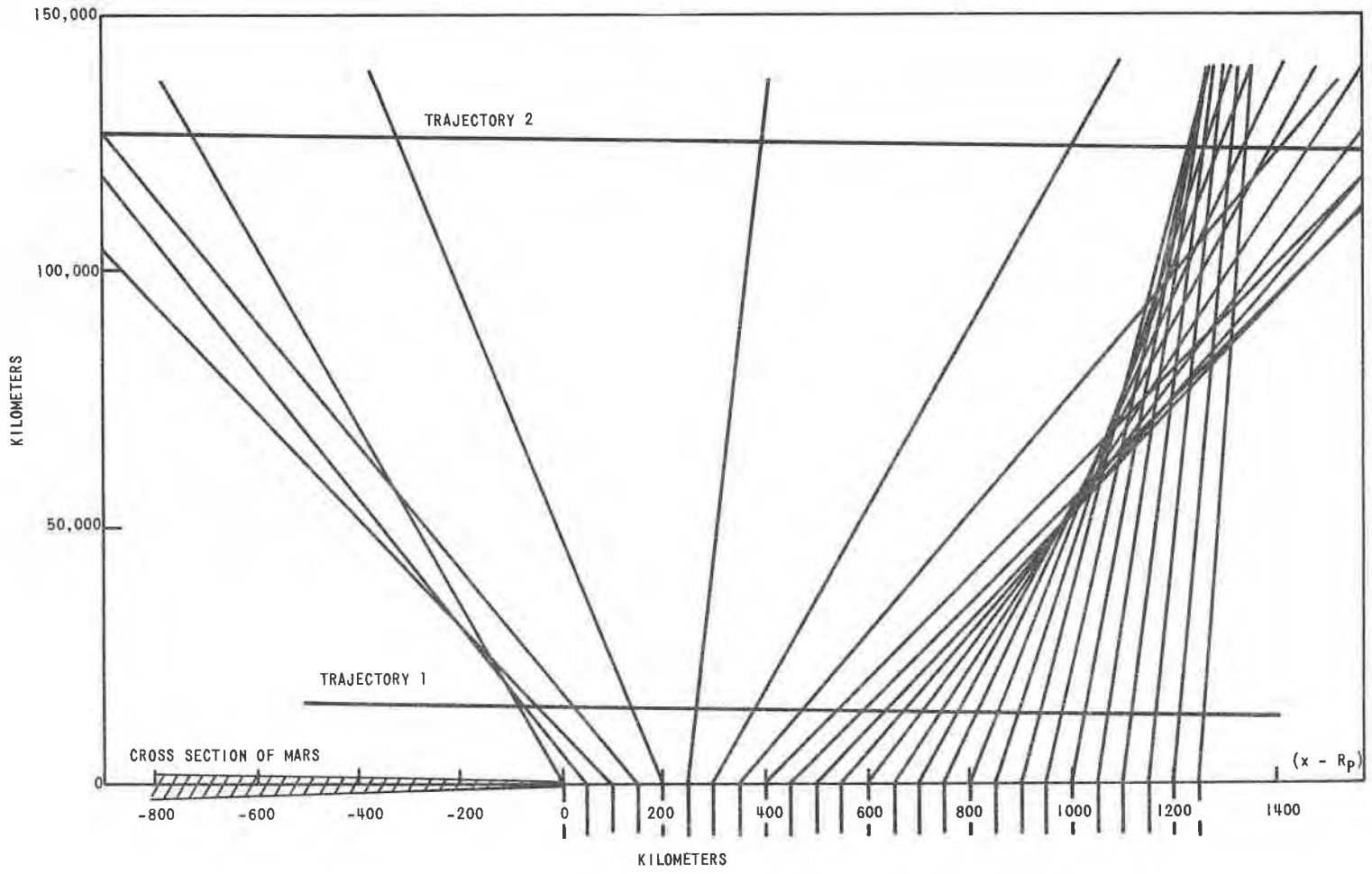

FIG. 20. REFRACTION IN A MARTIAN IONOSPHERE AT 50 Mc. (Assumed electron density: Chapman layer, H = 130 km, h_o = 320 km, $N_{max} = 10^{11}$ electrons/m^3, sec χ_o = 1.175.)

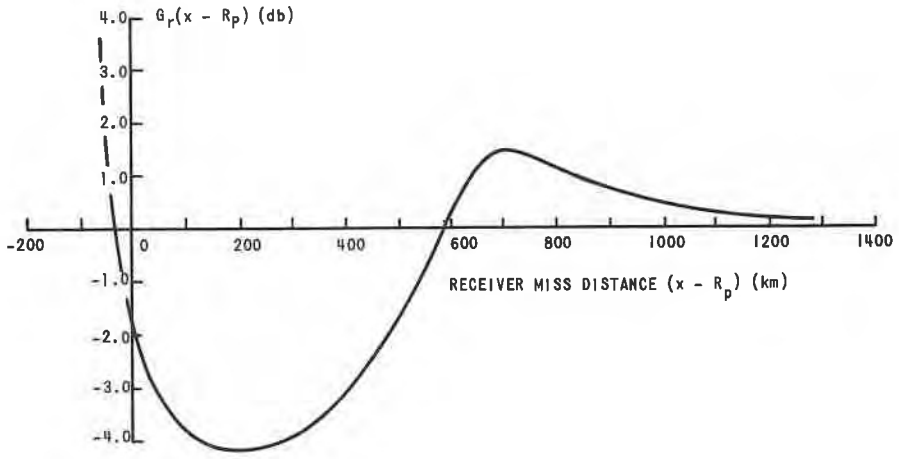

FIG. 21. REFRACTION GAIN $G_r(x-R_p)$ AT 50 Mc DURING OCCULTATION ALONG TRAJECTORY 1.

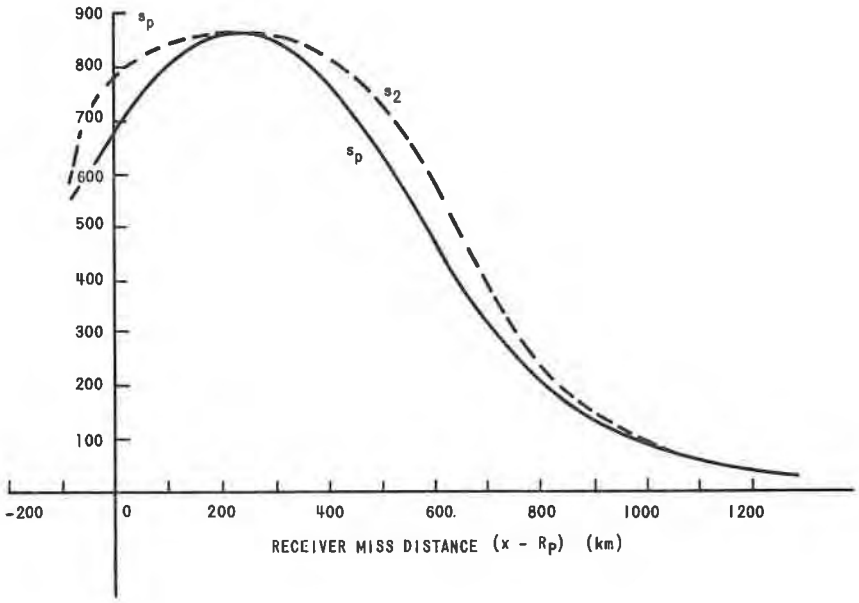

FIG. 22. DECREASE IN PHASE PATH (s_p) DUE TO THE MARTIAN IONOSPHERE (f = 50 Mc, TRAJECTORY 1).

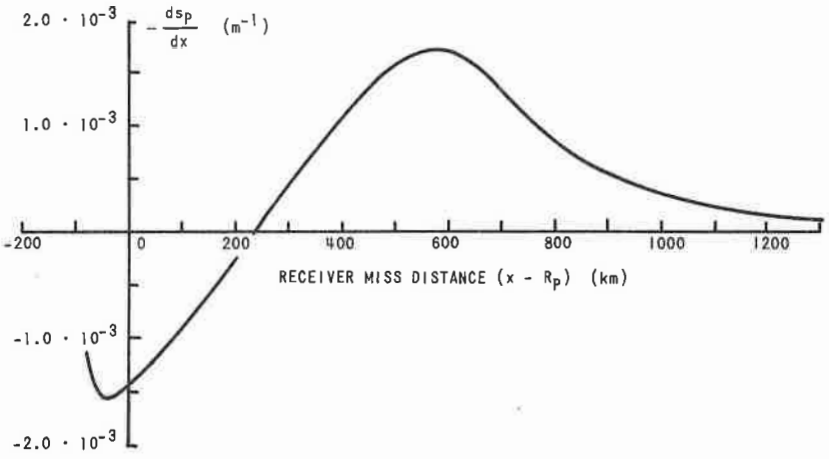

FIG. 23. RATE OF CHANGE IN PHASE-PATH DECREASE ds_p/dx FOR TRAJECTORY 1.

the Martian ionosphere causes a doppler shift of 1.7 cps at miss distance 600 km. As explained in Sec. IIB, this can be measured by comparing it with the eighth subharmonic of a 400-Mc signal.

The shape of the curves for phase path and refraction gain vs receiver miss distance depends strongly on the trajectory. Figures 24 and 25 show the results for trajectory 2. We see that the gain and the phase path now are multivalued functions of $(x - R_p)$. This is because the signal in certain regions is received over more than one propagation path at a time.

Trajectory 2 crosses two branches of the outer caustic at miss distances 1700 km and 1300 km, respectively. The inner caustic in this numeric example has only one branch in the x-y plane. This branch is encountered at miss distance -1100 km.

So far we have neglected the nonspherical variations in the electron density distribution. Taking these into account we find the changes shown in Figs. 26 and 27. The nonspherical ionosphere used here corresponds to Eq.(4.1) for $\chi \leq 85$ deg and

$$X\left(\frac{r_o}{\cos\alpha}, \chi\right) = X\left(\frac{r_o}{\cos\alpha}, 85 \text{ deg}\right) \qquad \text{for} \quad \chi > 85 \text{ deg}$$

[A modification of Eq. (4.1) is necessary because it is not valid for large χ.] The two ionospheres used in the comparison in Figs. 26 and 27 have the same electron density only along the x axis.

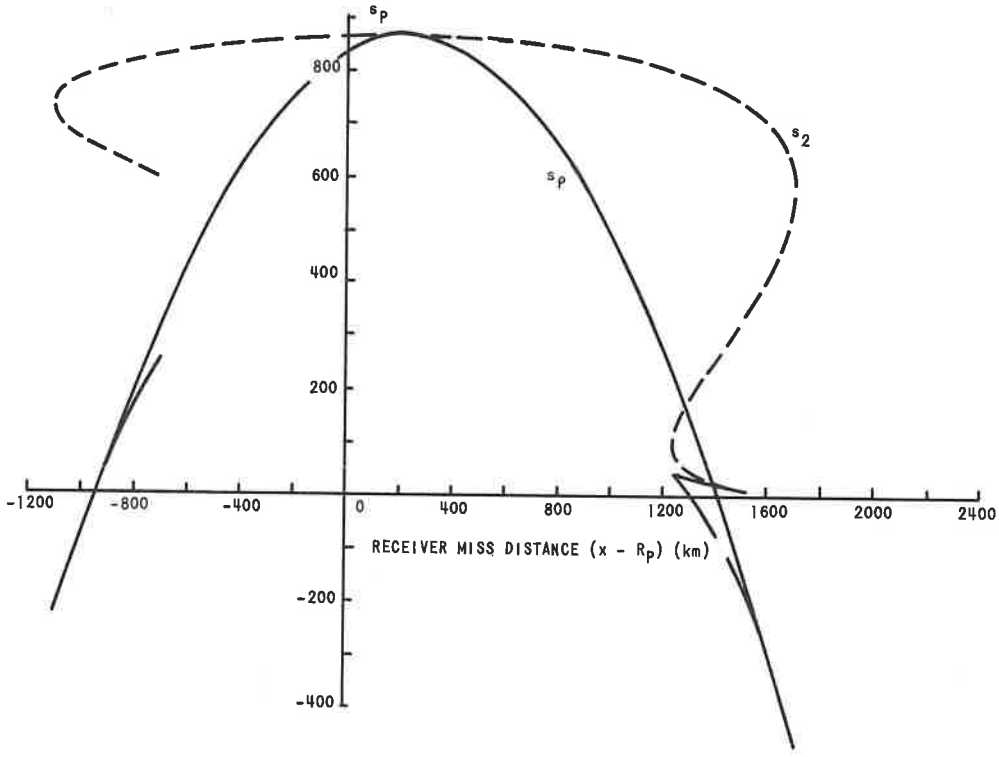

FIG. 24. DECREASE IN PHASE PATH (s_p) FOR TRAJECTORY 2.

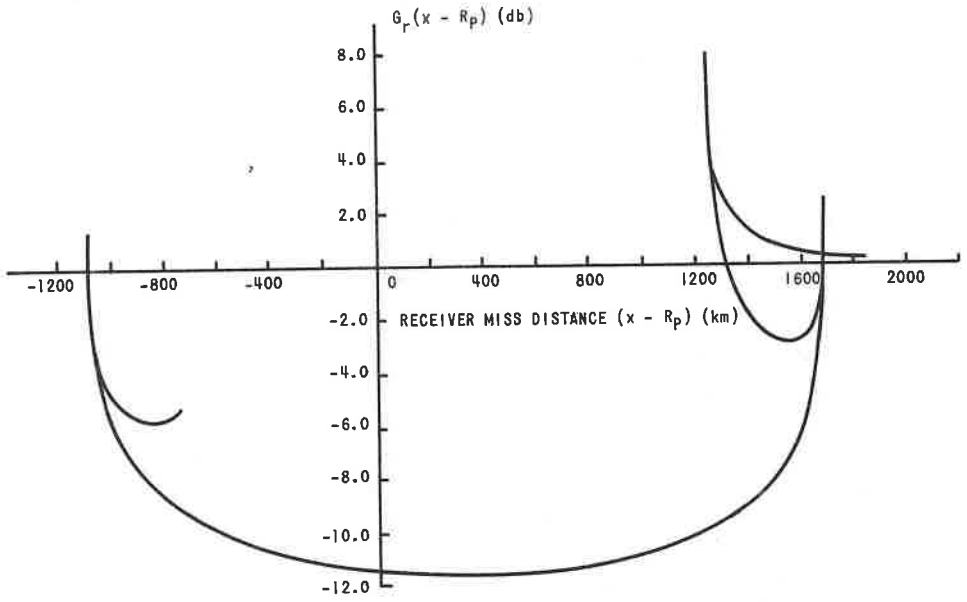

FIG. 25. REFRACTION GAIN $G_r(x-R_p)$ FOR TRAJECTORY 2.

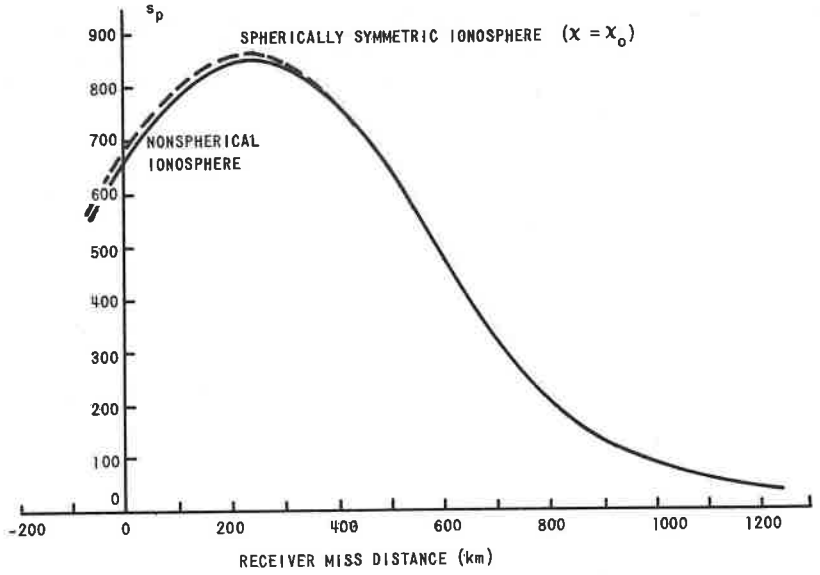

FIG. 26. EFFECT OF NONSPHERICAL PERTURBATIONS IN THE ELECTRON DENSITY DISTRIBUTION (s_p AT 50 Mc FOR TRAJECTORY 1).

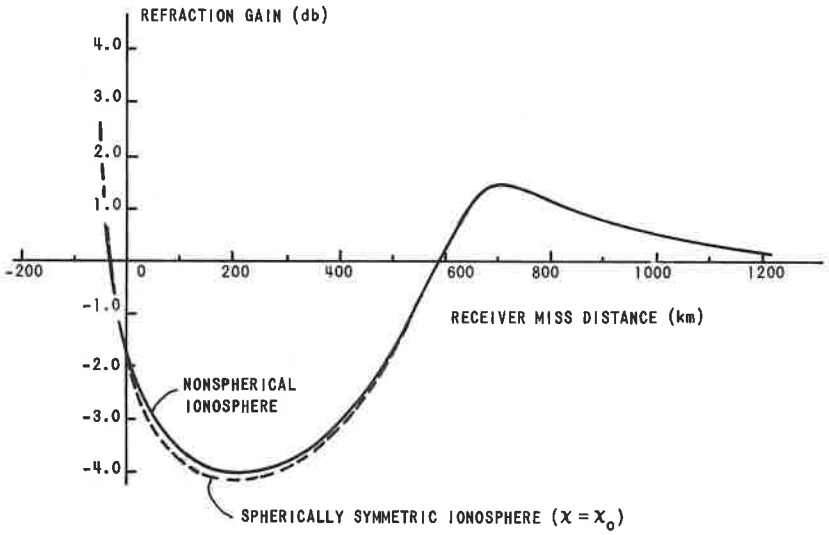

FIG. 27. EFFECT OF NONSPHERICAL PERTURBATIONS IN THE ELECTRON DENSITY DISTRIBUTION (REFRACTION GAIN AT 50 Mc FOR OCCULTATION ALONG TRAJECTORY 1).

V. DETERMINATION OF THE ELECTRON DENSITY DISTRIBUTION FROM AMPLITUDE, PHASE PATH, OR GROUP PATH

Previous chapters have discussed how to find amplitude, phase path, and group path of high-frequency radio waves propagating through a planetary ionosphere with known electron density profile. The purpose of an experiment would of course be to measure the gain $G_r(x)$, the changes in the phase path $s_p(x)$, or the changes in the group path $s_g(x)$ as the transmitter is occulted by the ionosphere, and from this, deduce the distribution of electron density for that part of the ionosphere which is probed by the waves reaching the receiver. In other words the problem has been reversed, but the results derived previously are still of great value.

Propagation through a nonspherical ionosphere can, as has been shown, be treated as if the ionosphere were spherically symmetric. We then use the same radial distribution of electron density in that part of the ionosphere which is probed by the signal, but variations in the electron density with longitude and latitude are neglected.

The equivalent trajectory (Fig. 1) comes in very handy here too; and we will assume that $G_r(x)$, $s_p(x)$, and $s_g(x)$ correspond to measurements along this trajectory.

The two first sections in this chapter are mainly devoted to studies of processes which can be used to find the angle of refraction $2\Psi(r_o)$ or the normalized straight-line integrated electron density $s_2(r_o)$ from $G_r(x)$, $s_p(x)$ or $s_g(x)$. Here x denotes the abscissa coordinate of the receiver and r_o the radius of closest approach for the raypath. (See Fig. 5.)

Later we show how the normalized electron density distribution $X(r)$ can be found from $s_2(r_o)$.

A. DETERMINATION OF THE NORMALIZED STRAIGHT-LINE INTEGRATED ELECTRON DENSITY $s_2(r_o)$ FROM THE REFRACTION GAIN $G_r(x)$

The refraction gain $G_r(x)$ along the equivalent trajectory is given by Eq. (2.33). We will assume that that part of the equivalent trajectory along which the occultation is observed can be approximated with a straight line:

$$y = y_o - ux \tag{5.1}$$

The same procedure can be employed when a piecewise linear approximation is used for the equivalent trajectory.

The radius of closest approach r_o for the ray that is crossing the receiver will be approximated by

$$r_o = x - (2\psi + \beta)\, y \tag{5.2}$$

where (x,y) are the receiver coordinates. This corresponds to setting r_o equal to $(R_p + q)$ in Fig. 5. We will further assume that $y \ll D$. The geometrical quantities used here are shown in Fig. 5.

Some remarks are also necessary on the notation we are going to use. A ray with radius of closest approach, r_o, is bent an angle $2\psi(r_o)$ which is a unique function of r_o. Since the rays in the x-y plane cross the equivalent trajectory, the same angle can also be considered a function of receiver abscissa x and we will then write $2\psi^*(x)$. Although $2\psi(r_o)$ and $2\psi^*(x)$ are equal when they refer to the same ray, it is still convenient to have some difference in the notation, especially since $2\psi^*(x)$ may be a multivalued function of x. For s_2 and β, we will similarly use $s_2(r_o)$, $s_2^*(x)$, $\beta(r_o)$, and $\beta^*(x)$. For $\beta(r_o)$ we have

$$\beta(r_o) \approx \frac{r_o}{D} \tag{5.3}$$

From Eq. (2.33) one can now obtain

$$\frac{d[2\psi^*(x) + \beta^*(x)]}{1 + u[2\psi^*(x) + \beta^*(x)]} = g(x)\, dx \tag{5.4}$$

where

$$g(x) = \frac{1}{y_o - ux}\left[1 \mp \frac{10^{G_r(x)/10}}{\left(1 + \frac{y_o - ux}{D}\right)\left(1 - 2\psi^*(x)\,\frac{y_o - ux}{x}\right)}\right] \tag{5.5}$$

The upper sign in Eq. (5.5) should be used when there is no caustic between the receiver and the planetary ionosphere; and the lower sign should be used when the rays have crossed each other somewhere between the receiver and the ionosphere. The expression for $g(x)$ can be simplified when the trajectory lies close behind the ionosphere.

Rewriting Eq. (5.4) in integral form and neglecting $u[2\psi^*(x) + \beta^*(x)]$, one obtains

$$2\psi^*(x) + \beta^*(x) - \beta^*(x_b) = \int_{x_b}^{x} g(x)\, dx \qquad (5.6)$$

where x_b corresponds to a position of the receiver before the occultation has started. At $x = x_b$ we have

$$\begin{aligned} G_r(x_b) &= 0 \\ 2\psi^*(x_b) &= 0 \\ \beta^*(x_b) &= \frac{x_b}{D + y_o - ux_b} \end{aligned} \qquad (5.7)$$

Equation (5.6) may at first appear to be useless because $g(x)$ depends on the unknown function $2\psi^*(x)$. However the term containing $2\psi^*(x)$ in the expression for $g(x)$ is small compared to 1 in the high-frequency case. This makes Eq. (5.6) a very useful tool for obtaining $2\psi^*(x)$.

Let us first look at a method that can be used to integrate Eq. (5.6) directly. The integration can be done by summing $-g(x)\,\Delta x$ from large toward smaller values of x. Let us assume that $2\psi^*(x)$ and $\beta^*(x)$ are found in the region from x_b to x (where x is less than x_b). The next step consists of determining $2\psi^*(x - \Delta x)$ and $\beta^*(x - \Delta x)$. One can calculate $g(x - \Delta x)$ using $2\psi^*(x)$ instead of $2\psi^*(x - \Delta x)$. This is possible because the term containing $2\psi^*(x)$ in Eq. (5.5) is small compared to 1. Equation (5.6) now gives $[2\psi^*(x - \Delta x) + \beta^*(x - \Delta x)]$, which again can be used to calculate the corresponding r_o by means of Eq. (5.2). Thus $\beta^*(x - \Delta x)$ can now be computed from Eq. (5.3). This also enables us to find $2\psi^*(x - \Delta x)$ since we already know $[2\psi^*(x - \Delta x) + \beta^*(x - \Delta x)]$. By repeating this procedure one obtains $2\psi^*(x)$ and $\beta^*(x)$ for all values of x where $G_r(x)$ is known. This method is well suited for use on a digital computer when $G_r(x)$ is known in sufficient detail.

Another way to approach this problem is to neglect $2\psi^*(x)$ in $g(x)$ as a first approximation. One then obtains

$$2\psi_1^*(x) + \beta_1^*(x) - \beta^*(x_b) = \int_{x_b}^{x} g_1(x)\, dx \tag{5.8}$$

where

$$g_1(x) = \frac{1}{y_o - ux}\left[1 \mp \frac{10^{G_r(x)/10}}{1 + \frac{y_o - ux}{D}}\right] \tag{5.9}$$

By using Eqs. (5.8), (5.2), and (5.3) one can now determine a first approximation $[2\psi_1^*(x)]$ for the angle of refraction $2\psi^*(x)$.

A second approximation $[2\psi_2^*(x)]$ for $2\psi^*(x)$ can be found by repeating this procedure. One obtains

$$2\psi_2^*(x) + \beta_2^*(x) - \beta^*(x_b) = \int_{x_b}^{x} g_2(x)\, dx \tag{5.10}$$

where

$$g_2(x) = \frac{1}{y_o - ux}\left\{1 \mp \frac{10^{G_r(x)/10}}{\left(1 + \frac{y_o - ux}{D}\right)\left[1 - 2\psi_1^*(x)\,\frac{y_o - ux}{x}\right]}\right\} \tag{5.11}$$

This iterative process can be employed until sufficient accuracy is obtained for $2\psi^*(x)$ and $\beta^*(x)$.

The functions $G_r(x)$, $g(x)$ and $[2\psi^*(x) + \beta^*(x)]$ are multivalued functions of x when the rays cross each other somewhere between the receiver and the planetary ionosphere. Figure 28 illustrates how $[2\psi^*(x) + \beta^*(x) - \beta^*(x_b)]$ is obtained from integration along the branches of $g(x)$. The poles in $g(x)$ coincide with the poles in $G_r(x)$, and they lie where the trajectory crosses caustics. However, the amplitude never goes to infinity at caustics such as $G_r(x)$ predicts. (See Appendix A.) Thus the true gain $G_T(x)$ does not have any poles. One can therefore not expect to obtain an accurate determination of $[2\psi^*(x) + \beta^*(x) - \beta^*(x_b)]$ by substituting $G_T(x)$ for $G_r(x)$ when the trajectory is crossing one or more caustics. However if the detailed

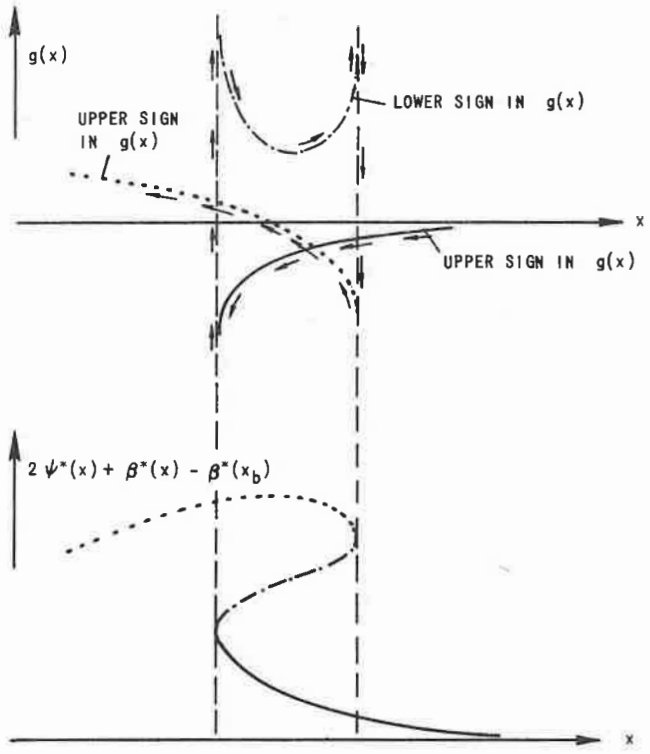

FIG. 28. INTEGRATION OF EQ. (5.6).

behavior of $G_T(x)$ is known around the caustics, one may from this estimate the corresponding ray theory gain $G_r(x)$ and thereby improve the accuracy. (Multipath propagation can be avoided by choosing the frequency high enough such that the caustics will lie behind the spacecraft trajectory. Estimates can be made by using the results derived in Chapters III and IV.)

The next step in the process of obtaining $s_2(r_o)$ from $G_r(x)$ consists of finding $2\psi(r_o)$. This is done by changing the variable from x to r_o using Eq. (5.2).

Finally, Eq. (2.28) relates $2\psi(r_o)$ and $s_2(r_o)$. Thus,

$$s_2(r_o) = \frac{f}{c}\int_{r_o}^{\infty} 2\psi(r_o)\, dr_o \qquad (5.12)$$

We have now seen how $s_2(r_o)$ can be deduced from the refraction gain $G_r(x)$. The function $s_2(r_o)$ is only related to that part of the ionosphere through which the signal is propagating; and we have therefore eliminated the dependence upon the particular trajectory along which the measurements happen to be made.

The next section shows that $s_p(x)$ or $s_g(x)$ also can be used to obtain $s_2(r_o)$ in the high-frequency case.

The radial distribution in electron density $X(r)$ in that part of the ionosphere which is probed by the signal, can be determined from $s_2(r_o)$. (See Secs. C and D.)

Losses due to electron collisions cause absorption at lower frequencies. This absorption coefficient is proportional to the product of collision frequency and X [Ref. 8]. One may, by observing the amplitude at different frequencies, be able to determine the radial variation in the collision frequency (if the data are good enough). The highest frequency would yield $X(r)$ and this enables us to compute the refraction gain at the lowest frequency. The difference between the observed gain and the computed refraction gain at the lowest frequency yields the radial variations in the straight-line integrated absorption coefficient. The problem of finding the radial variation in collision frequency is analogous to determining $X(r)$ from $s_2(r_o)$. Sections C and D can therefore be used in both cases.

B. DETERMINATION OF THE NORMALIZED STRAIGHT-LINE INTEGRATED ELECTRON DENSITY $s_2(r_o)$ FROM THE PHASE PATH $s_p(x)$ OR THE GROUP PATH $s_g(x)$

The only difference between the form of $s_p(x)$ and $s_g(x)$ is a difference in sign in front of s_1. [See Eqs. (2.20) and (2.23).] We shall first look at a method in which this sign difference is of no importance as far as the determination of $s_2(r_o)$ goes. We will use $s_p(x)$ here but the method also applies to $s_g(x)$.

Equation (2.20) gives

$$-s_1(x) + s_2^*(x) = s_p(x) \tag{5.13}$$

where the * again is used to emphasize that s_2 here is considered a function of the receiver abscissa x. One can neglect $s_1(x)$ when the

receiver is flying close to the planetary ionosphere. Thus as a first approximation $s_{21}(r_o)$ to $s_2(r_o)$, one obtains:

$$s_{21}(r_o) = s_p(r_o) \tag{5.14}$$

where the receiver abscissa x is simply replaced by the radius of closest approach r_o for the ray that crosses the receiver. The first approximation in $2\psi_1(r_o)$ can now be determined from Eq. (2.28).

The function $s_{21}(r_o)$ may not be a sufficiently accurate approximation to $s_2(r_o)$, but this approximation can be improved by repeated use of Eq. (5.13). For instance, when the waves can be considered plane before they are refracted in the planetary ionosphere, this gives:

$$s_{22}(r_o) = s_p(x) + \frac{f}{c}(x - r_o)\,\psi_1(r_o) \tag{5.15}$$

This equation is obtained by combining Eqs. (5.13) and (2.24). The term Δs_1 in Eq. (2.24) has been neglected and so has the difference between a and r_o. When the receiver trajectory is given by Eq. (5.1), one can show that

$$x = \frac{r_o + y_o\, 2\psi_1(r_o)}{1 + u\, 2\psi_1(r_o)}$$

This enables us to determine the second approximation $s_{22}(r_o)$ of $s_2(r_o)$ from Eq. (5.15).

Higher order corrections to $s_2(r_o)$ can be found by repeating this procedure.

Another way to approach the problem is to consider the slope of $s_p(x)$. For $\left|2u\,\frac{c}{f}\,\frac{ds_p}{dx}\right| \ll 1$, one can show that

$$2\psi^*(x) = -\frac{c}{f}\,\frac{ds_p(x)}{dx} \tag{5.16}$$

where $2\psi^*(x)$ denotes the angle of refraction as a function of receiver abscissa x. This equation can be considered a generalization of Eq. (2.28). Once $2\psi^*(x)$ is determined from Eq. (5.16), one can use the method explained in Sec. VA to find $s_2(r_o)$. [Equation (5.16) does not apply to $s_g(x)$.]

Other ways to determine $s_2(r_o)$ have been found during this study. However, they are believed to be of less importance and are therefore not given here.

We have shown that either the phase path, the group path, or the amplitude can be used to obtain $s_2(r_o)$. However, it may be an advantage to make two of these measurements simultaneously in order to reduce experimental errors and possible uncertainties introduced by variations in the medium between the transmitter and the planetary ionosphere. Ambiguities can also be avoided by receiving on several frequencies in the spacecraft.

C. DERIVATION OF A RECURSIVE FORMULA RELATING THE NORMALIZED ELECTRON DENSITY DISTRIBUTION $X(r)$ TO THE NORMALIZED STRAIGHT-LINE INTEGRATED ELECTRON DENSITY $s_2(r_o)$

It was shown in the two previous sections how $G_r(x)$, $s_p(x)$, or $s_g(x)$ can be used to obtain $s_2(r_o)$. In this and the next section we will show how to determine the normalized electron density distribution $X(r)$ from $s_2(r_o)$.

In this section the coordinate system shown in Fig. 29 is used. Let us consider the planetary ionosphere built up of K spherical layers with constant electron density in each. Equation (2.27) can now be rewritten in the following form:

$$2 \frac{c}{f} s_2(m) = X(m) \Delta y(m,m) + 2\sum_{n=1}^{m-1} X(n) \Delta y(m,n) \qquad (5.17)$$

Here s_2 is denoted $s_2(m)$ for the m^{th} ray and $X(n)$ is the normalized electron density in the n^{th} layer. In Fig. 29, $\Delta y(m,n)$ designates the line element corresponding to the n^{th} layer and the m^{th} ray. From Eq. (5.17),

$$X(1) = \frac{2 \frac{c}{f} s_2(1)}{\Delta y(1,1)}$$

$$X(2) = \frac{2 \frac{c}{f} s_2(2) - 2\sum_{n=1}^{1} X(n) \Delta y(2,n)}{\Delta y(2,2)}$$

. .
. .
. .

$$X(m) = \frac{2\,\frac{c}{f}\,s_2(m) - 2\sum_{n=1}^{m-1} X(n)\,\Delta y(m,n)}{\Delta y(m,m)} \tag{5.18}$$

which provides us with a recursive formula relating X to s_2.

The two-dimensional matrix Δy can be expressed in terms of the radii of the spherical layers:

$$\Delta y(m,n) = \left[r_n^2 - \left(\frac{r_m + r_{m+1}}{2}\right)^2\right]^{1/2} - \left[r_{n+1}^2 + \left(\frac{r_m + r_{m+1}}{2}\right)^2\right]^{1/2} \tag{5.19}$$

for $m > n$, and

$$\Delta y(m,m) = 2\left[r_m^2 - \left(\frac{r_m + r_{m+1}}{2}\right)^2\right]^{1/2} \tag{5.20}$$

for $n = m$.

It turns out that these results can be extended to include a special case where the ionosphere is not spherically symmetric. Although this case is not of much importance in this context, it may clarify the inversion process and will therefore be included.

Let X be a separable function of the radial distance to the center of the planet r and of the solar zenith angle χ:

$$X(r,\chi) = X_1(r)\,A(\chi)$$

Using $A(m,n)$ and $A'(m,n)$ to denote the solar zenith angles for the line elements $\Delta y(m,n)$ above and below the x axis respectively, one finds

$$X_1(m) = \frac{2\,\frac{c}{f}\,s_2(m) - \sum_{n=1}^{m-1} X_1(n)\,\Delta y(m,n)[A(m,n) + A'(m,n)]}{\Delta y(m,m)\,A(m,m)} \tag{5.21}$$

which shows that it is necessary to know $A(\chi)$ in order to find $X_1(r)$.

Another convenient method for calculation of $X(r)$ from $s_2(r_o)$ is given in the next section.

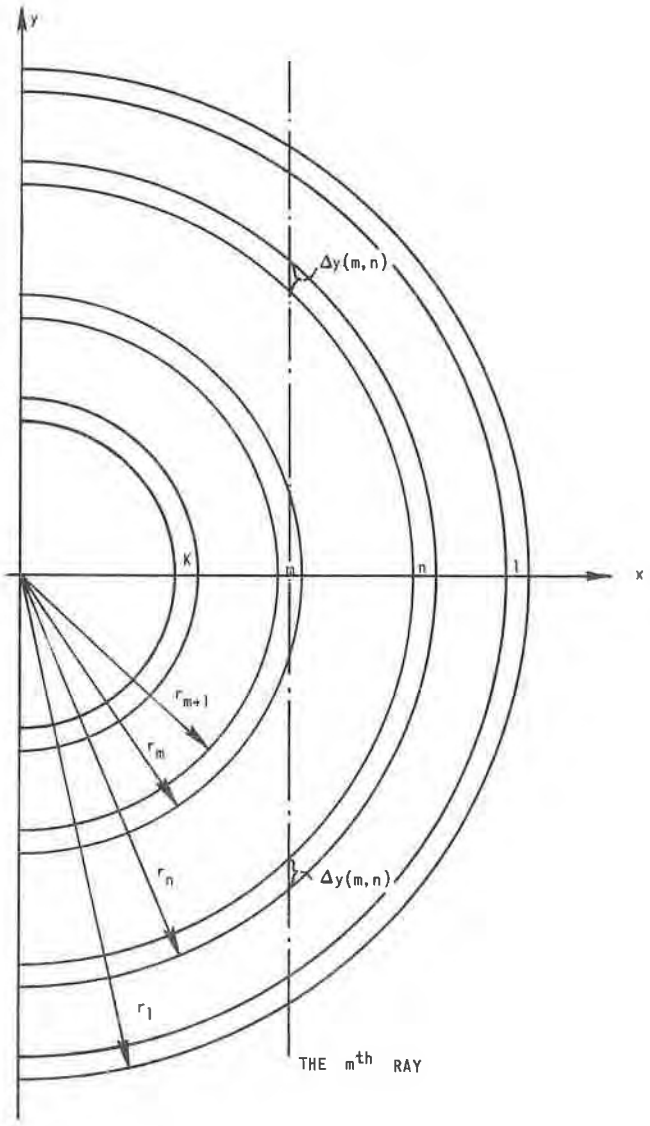

FIG. 29. IONOSPHERE CONSISTING OF K SPHERICAL LAYERS.

D. APPLICATION OF THE ABELIAN INTEGRAL EQUATION TO THE DETERMINATION OF THE NORMALIZED ELECTRON DENSITY DISTRIBUTION $X(r)$ FROM THE NORMALIZED STRAIGHT-LINE INTEGRATED ELECTRON DENSITY $s_2(r_o)$

Equation (2.27) is a special case of an integral equation solved by Abel. His results can be found in most textbooks on the subject [Ref. 9].

Changing the variable of integration in Eq. (2.27) gives

$$\frac{c}{f}\, s_2(r_o) = \int_{r_o}^{\infty} X(r) \left[1 - \left(\frac{r_o}{r}\right)^2\right]^{-1/2} dr \qquad (5.22)$$

where r is given by Eq. (2.9). By using $1/r^2$ as a dummy variable of integration in Eq. (5.22), one can obtain from comparison with Abel's solution:

$$X(r) = \frac{2}{\pi}\frac{c}{f}\frac{d}{dr}\left\{\int_{r_o=\infty}^{r} \frac{s_2(r_o)}{r_o} \left[\left(\frac{r_o}{r}\right)^2 - 1\right]^{-1/2} dr_o\right\} \qquad (5.23)$$

This is the formal solution to the problem, but it is not a very convenient solution from the point of view of numerical analysis. It is therefore tempting to try to modify Eq. (5.23). One can show, after differentiation with respect to r, that:

$$X(r) = \frac{2}{\pi}\frac{c}{f}\int_{r}^{\infty} [s_2(r) - s_2(r_o)]\, r_o (r_o^2 - r^2)^{-3/2}\, dr_o \qquad (5.24)$$

This form of the integrand cannot be evaluated accurately close to the lower limit r. Expanding the integrand in the interval r to $r + \Delta r$ gives:

$$X(r) = -\frac{2}{\pi}\frac{c}{f}\frac{ds_2(r)}{dr}\left(\frac{\Delta r}{2r}\right)^{1/2} + \frac{2}{\pi}\frac{c}{f}\int_{r+\Delta r}^{\infty} [s_2(r) - s_2(r_o)]\, (r_o^2 - r^2)^{-3/2}\, r_o dr_o \qquad (5.25)$$

where Δr should be small enough so that $s_2(r_o)$ can be approximated accurately by $s_2(r) + [ds_2(r)/dr](r_o - r)$. It is also assumed that $\Delta r \ll r$.

The function $s_2(r_o)$ in the integrand of Eq. (5.25) decreases rapidly with increasing r_o, but $r_o(r_o^2 - r^2)^{-3/2}$ does not. Therefore, in order to cut down the computation time, one can modify the integral in the following manner. Let

$$s_2(r_o) = 0 \qquad \text{for} \quad r_o > r_b$$

Splitting up the integration in two new intervals $(r + \Delta r, r_b)$ and (r_b, ∞) gives

$$X(r) = -\frac{2}{\pi}\frac{c}{f}\frac{ds_2(r)}{dr}\left(\frac{\Delta r}{2r}\right)^{1/2} + \frac{2}{\pi}\frac{c}{f}\int_{r+\Delta r}^{r_b}[s_2(r) - s_2(r_o)]$$

$$\cdot(r_o^2 - r^2)^{-3/2}\, r_o dr_o + \frac{2}{\pi}\frac{c}{f}\, s_2(r)(r_b^2 - r^2)^{-1/2} \qquad (5.26)$$

and this form is very well suited for use on a digital computer.

We have now discussed procedures which can be used to obtain the normalized electron density profile $X(r)$ from measurements of changes in the amplitude, the phase path, or the group path during occultation. Because of the complexity of the methods and the many approximations involved, it appears almost impossible to carry out any general analysis of the final errors in $X(r)$. However, let us briefly look at the simplest case where refraction is negligible so that $s_2(r_o)$ can be determined directly from phase-or group-path measurements. We will use $s_{2E}(r_o)$ to denote the error in $s_2(r_o)$, and $X_E(r)$ to denote the corresponding error in $X(r)$. One can show that $X_E(r)$ is given by Eq. (5.26) when $s_2(r_o)$ is replaced by $s_{2E}(r_o)$ [and $X(r)$, by $X_E(r)$]. [Errors in $s_2(r_o)$ for $r_o > r_b$ do not influence the final result when Eq. (5.26) is used in the inversion process.] Equation (5.26) can be simplified when $s_{2E}(r_o)$ can be considered as varying rapidly around zero so that

$$\frac{2}{\pi}\frac{c}{f}\int_{r+\Delta r}^{r_b} - s_{2E}(r_o)(r_o^2 - r^2)^{-3/2}\, r_o dr_o$$

may be neglected. One then obtains for the absolute error in $X(r)$:

$$X_E(r) \approx \frac{2}{\pi}\frac{c}{f}\left[-\frac{ds_{2E}(r)}{dr}\Delta r + s_{2E}(r)\right](2r\Delta r)^{-1/2}$$

showing that the error in X at r in this case only depends on $s_{2E}(r)$ around r. In order to determine the standard deviation in $X_E(r)$, it would be necessary to assume a probability distribution for $s_{2E}(r)$ and $ds_{2E}(r)/dr$.

The experimental errors may be the largest errors, but we also like to check the approximations we have developed. A complete numerical example is therefore worked out in the next section. This example may also clarify some of the previous derivations.

E. NUMERIC EXAMPLE

A numeric example was given in Sec. IVD, where it was shown how amplitude and phase may vary during an occultation. In particular, Fig. 21 shows $G_r(x - R_p)$ for trajectory 1.

We will now use, as an example, the gain shown in Fig. 21 and from this try to determine the corresponding electron density distribution in the Martian ionosphere. In doing so, we will make use of the results developed in Secs. VA and VD.

Equation (5.9) and Fig. 21 can be used to determine $g_1(x)$. We note that $1/D$ and β in Eqs. (5.9) and (5.8) are both zero in this example because in Sec. IVD we neglected the curvature of the wavefronts before refraction in the Martian ionosphere. (The quantities D and β are defined in Fig. 5.) The result of computing $g_1(x)$ is shown in Fig. 30 where $x - R_p$ is the receiver miss distance as viewed from the earth.

Integration of Eq. (5.8), where $g_1(x)$ is taken from Fig. 30, gives $2\psi_1^*(x)$ as shown in Fig. 31.

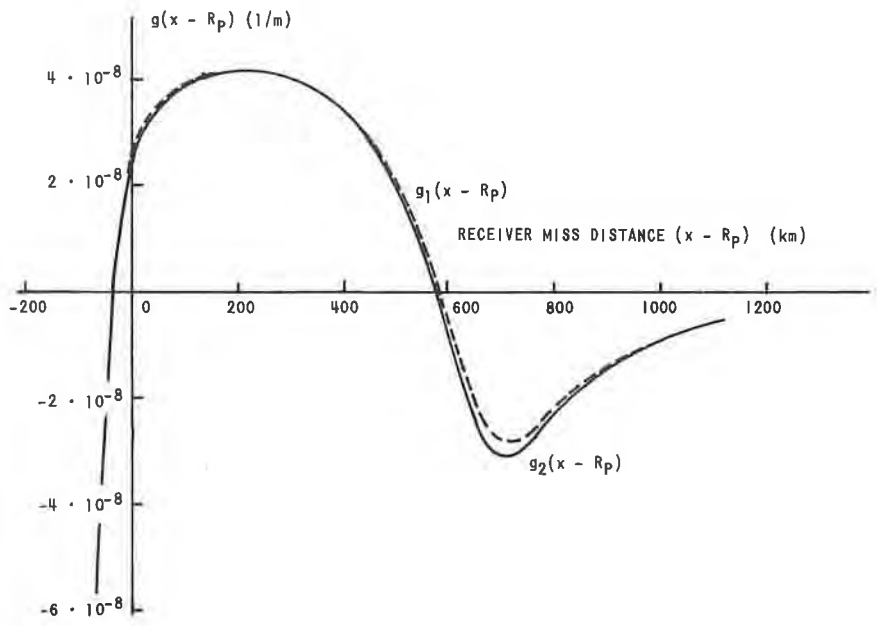

FIG. 30. THE FUNCTION $g(x-R_p)$ FOR TRAJECTORY 1.

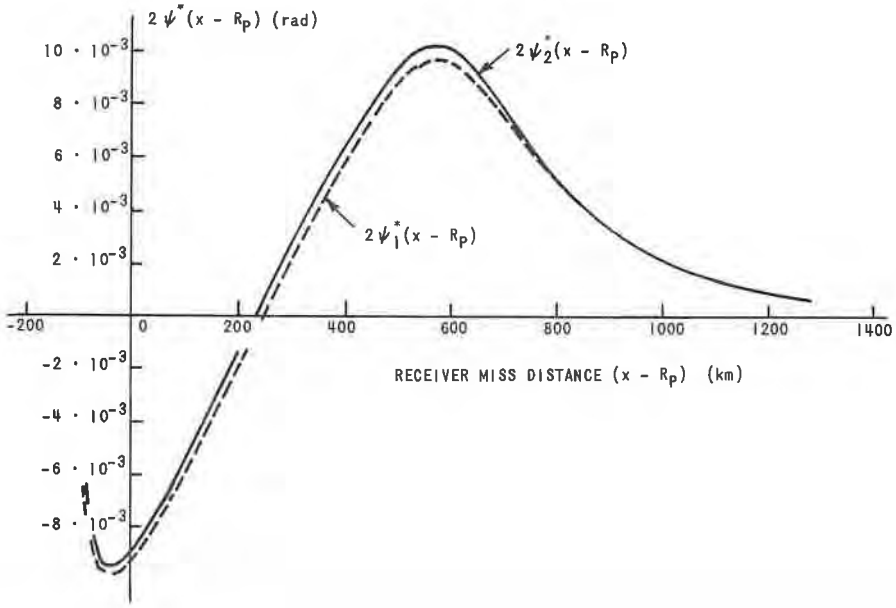

FIG. 31. THE FUNCTION $2\psi^*(x-R_p)$ FOR TRAJECTORY 1.

This procedure can now be repeated. By using Eqs. (5.11) and (5.10), we obtain $g_2(x)$ and $2\psi_2^*(x)$. The result is shown in Figs. 30 and 31.

Neglecting the difference between $2\psi_2^*(x)$ and $2\psi^*(x)$, we can now determine $2\psi(r_o)$ by means of Eq. (5.2). The result of this nonlinear scale transformation is shown in Fig. 32.

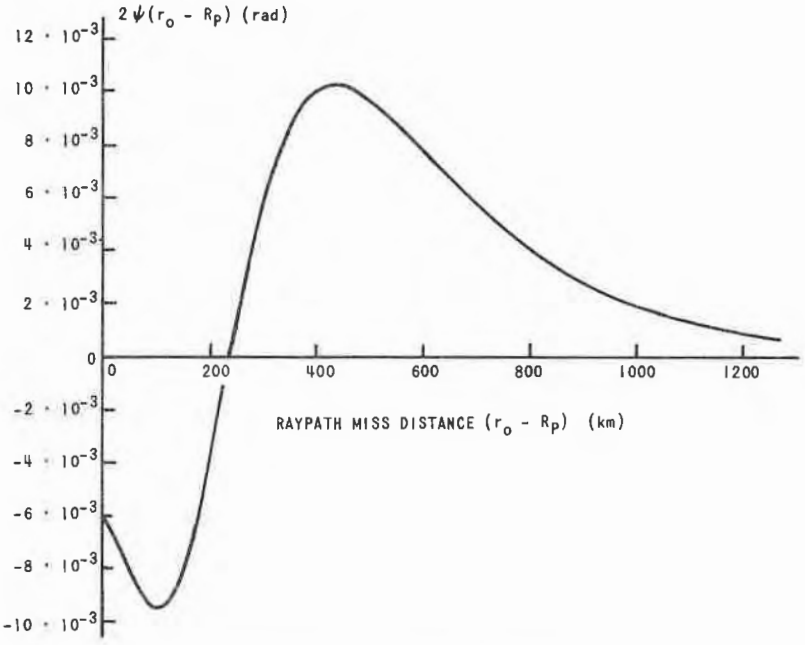

FIG. 32. THE FUNCTION $2\psi\ (r_o - R_p)$ AT 50 Mc FOR A MARTIAN IONOSPHERE.

The next step consists of determination of $s_2(r_o)$. By using Eq. (5.12), one obtains the result shown in Fig. 33.

Finally, Eq. (5.26) gives the electron density distribution that is causing the gain fluctuations in Fig. 21. The calculated points are plotted in Fig. 34, together with a curve representing the Chapman model originally assumed in Sec. IVD (Fig. 19). The agreement between the assumed and the calculated electron density distribution is good in spite of the many approximations involved.

Looking at both Secs. IVD and VE, we see that we have ended where we started, namely with the electron density distribution. When the data from an occultation experiment become available, it may be useful to check the result with a similar loop:

1. Use the data to determine the electron density distribution, then
2. Use the electron density distribution and calculate the quantities that were measured during the occultation.

Note that the last step can easily be carried beyond the first-order approximation (high-frequency approximation), while the first step cannot.

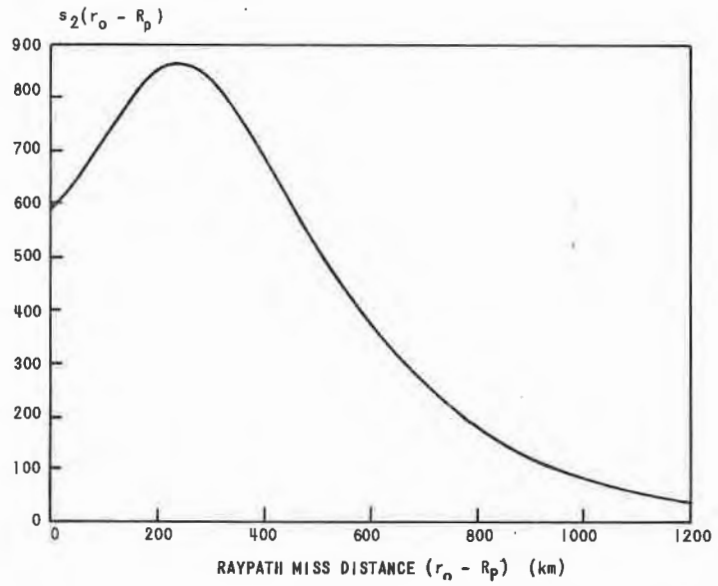

FIG. 33. THE FUNCTION $s_2(r_o - R_p)$ AT 50 Mc FOR A MARTIAN IONOSPHERE.

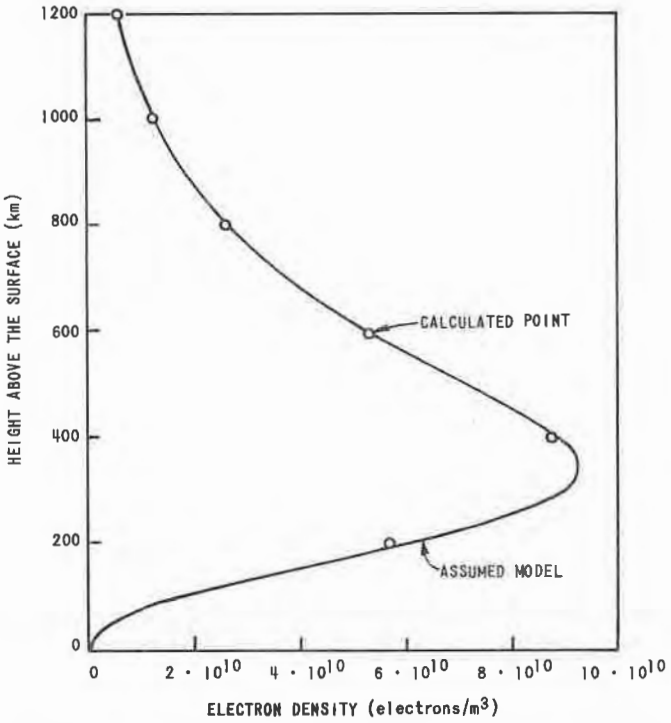

FIG. 34. COMPARISON BETWEEN ASSUMED AND CALCULATED ELECTRON DENSITY PROFILES.

F. OTHER ALTERNATIVES

In the previous sections we have seen some methods that can be used to determine the electron density distribution from measurement of amplitude, phase path, or group path. However, the methods are laborious, and it may turn out that the data, when available really will not qualify for this type of procedure. In other words, it may be that the uncertainties will be so large that, even after careful smoothing, the data may yield an unrealistic electron density distribution. In this case it may be better to determine characteristic properties of the ionosphere by comparing the data with the results obtained in Chapter III or Chapter IV. From this it may be possible, for instance, to determine upper and lower limits for the parameters of a Chapman-model ionosphere that will yield amplitude, phase path, or group path in agreement with the measurements.

Faraday rotation is another quantity that can be measured as mentioned in the introduction to Chapter II. One can show, when the quasi-longitudinal approximation applies, that the Faraday rotation is proportional to the integral along the raypath of X times the longitudinal component of the magnetic field [Ref. 10]. This yields a means of exploring the planetary magnetic field. However, assuming that the magnetic field around the planet may be considered a dipole field, one may also use the Faraday rotation to check or improve $X(r)$ found from phase or amplitude. The dipole field is uniquely specified by three numbers (two angles and the dipole moment), and the rest of the information contained in the Faraday rotation vs miss distance curve is therefore on $X(r)$.

So far we have studied radio-wave propagation through planetary atmospheres and ionospheres. It is also necessary to consider the waves reflected from the surface of the planet. The next chapter will deal with this problem.

VI. REFLECTION OF RADIO WAVES FROM PLANETARY SURFACES

Section IVD shows how amplitude and phase may vary for a signal propagating through a Martian ionosphere; however, waves will also be reflected from the surface of Mars. Let us therefore, in order to complete the example in Sec. IVD, briefly consider the reflected signal. Figure 35 shows the ray picture around the limb of Mars, assuming a smooth surface. It is clear from this picture that the intensity of the reflected signal will be way below the intensity of the direct propagating signal both along trajectory 1 and along trajectory 2. (See Fig. 18.) It therefore appears easy to distinguish the direct traveling wave from the wave reflected from the surface. This preliminary conclusion is based on the simple model used in Fig. 35. However, a more detailed study in the next sections will show essentially the same result.

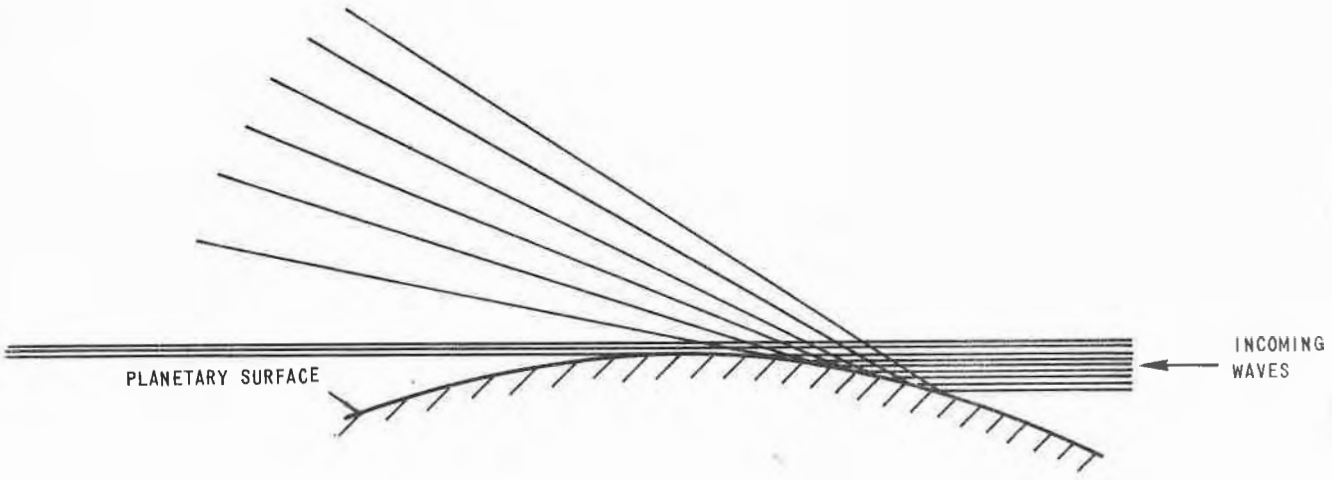

FIG. 35. REFLECTION FROM A SMOOTH, PERFECTLY REFLECTING PLANETARY SURFACE.

A. APPLICATION OF HUYGENS-KIRCHHOFF PRINCIPLE

The balance of this chapter considers radio waves transmitted from the earth and reflected from a rough planetary surface. A receiver is flying by the planet. The planetary surface is moving relative to the receiver, and this motion will impose a phase modulation on the reflected signal.

Many authors have studied radio-wave reflections from the moon and planets for the monostatic case in which both transmitter and receiver are situated on the earth [Refs. 11, 12, 13]. Here we will extend some of this work for use in the case where the transmitter is on the earth and the receiver is in a spacecraft flying by the planet (bistatic radar). The geometry at time t is illustrated in Fig. 36. The

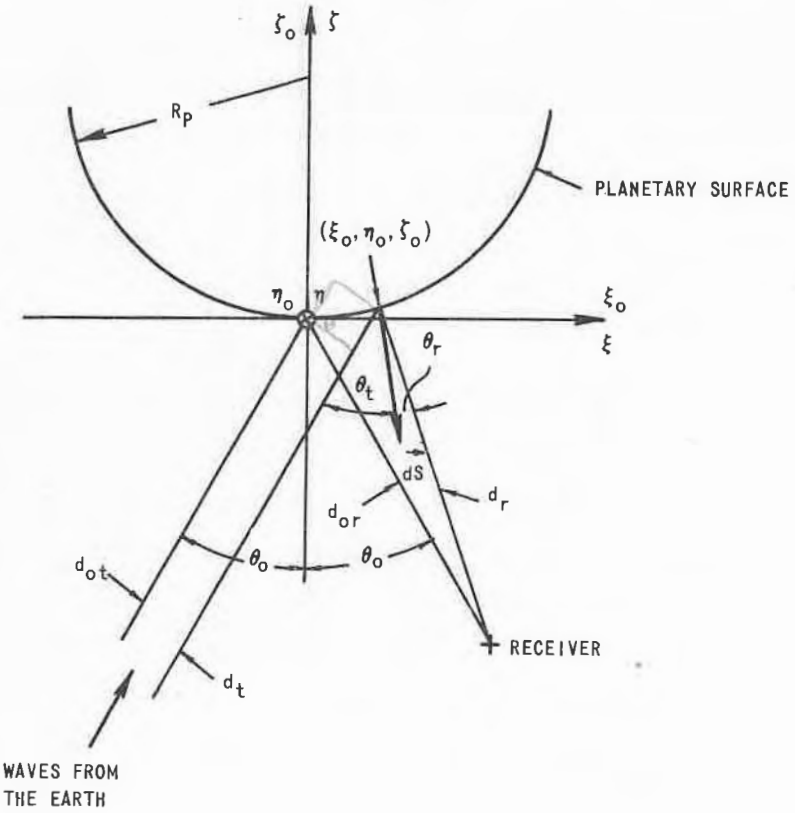

FIG. 36. GEOMETRY OF THE PROPAGATION PATH AT TIME t.

$\xi_o\eta_o\zeta_o$-coordinate system is chosen with the origin in the center of the first Fresnel zone and both the ξ_o and the η_o axes are tangential to the mean planetary surface. The $\xi_o\eta_o\zeta_o$-coordinate system is moving relative to the surface such that its origin always remains in the center of the first Fresnel zone. We also need a coordinate system that is fixed to the surface. Let us call its axes ξ, η, and ζ. The last coordinate system coincides with the $\xi_o\eta_o\zeta_o$-coordinate system at time t as shown in Fig. 36.

We will apply the Huygens-Kirchhoff principle in order to try to relate the statistics of the reflected signal to the statistics of the planetary surface. In order to do that, we need an expression for the phase of the signal reflected from a point on the planetary surface. Figure 37 shows a point (ξ_o, η_o, ζ_o) on the mean planetary surface. The reflection takes place on the surface at a distance $h(\xi_o, \eta_o, t)$ below the mean surface. It is necessary to make approximations in the expression for the phase path. Assuming that $h(\xi_o, \eta_o, t)$ is small compared to the other dimensions involved, one obtains for the phase path between the transmitter, the reflection point, and the receiver,

$$k(d_r + d_t) \approx k\left[d_{or} + d_{ot} + \frac{\xi_o^2}{2}\left(\frac{\cos^2\theta_o}{d_{or}} + \frac{\cos^2\theta_o}{d_{ot}} + \frac{2\cos\theta_o}{R_p}\right)\right.$$

$$\left. + \frac{\eta_o^2}{2}\left(\frac{1}{d_{or}} + \frac{1}{d_{ot}} + \frac{2\cos\theta_o}{R_p}\right) + 2h\cos\theta_o\right] \qquad (6.1)$$

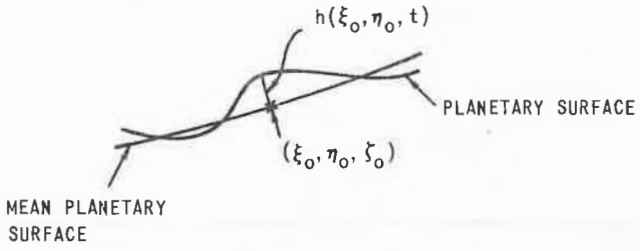

FIG. 37. CROSS SECTION OF SURFACE FEATURE.

For a flat surface (Spencer) with h << d_{or}, d_{ot}

$$k(d_r + d_t) \approx k\left[d_{or} + d_{ot} + \frac{\xi_o^2 + \eta_o^2}{2}\left(\frac{1}{d_{or}} + \frac{1}{d_{ot}}\right) + 2h\cos\theta_o\right]$$

where k is the free-space wave number, R_p is the mean planetary radius, θ_o is the angle of incidence at the origin, and d_{or} and d_{ot} are the distances between the origin, the receiver, and the transmitter, respectively. Only the first-order terms are maintained in Eq. (6.1). We have also neglected the effect of the ionosphere because this only causes a constant phase shift when the ionospheric contribution is independent of the position on the surface where the reflection takes place.

Let E_t be the amplitude at unit distance of the electric field of the transmitter. The Huygens-Kirchhoff principle then gives for the amplitude of the reflected wave at the receiver:

$$E_r(t) = \frac{ikE_t}{4\pi} \iint \exp\{i[\omega t - k(d_t + d_r)]\}(\cos\theta_t + \cos\theta_r)\frac{dS}{d_t d_r} \qquad (6.2)$$

where θ_t and θ_r are the angles that the normal to the surface element dS makes with d_t and d_r, respectively. The Huygens-Kirchhoff principle applies when the surface does not have any roughness scale comparable to the wavelength.

Equation (6.2) can be simplified by neglecting the variation in the distance and obliquity factors over the region of the surface contributing to the reflected signal. This simplification gives

$$E_r(t) \approx \frac{ikE_t \cos\theta_o}{2\pi d_{or} d_{ot}} \int_{-\infty}^{+\infty}\int_{-\infty}^{+\infty} \exp\{i[\omega t - k(d_t + d_r)]\}\, d\xi_o\, d\eta_o \qquad (6.3)$$

where the limits in the integration have been set equal to $\pm\infty$. This is valid when a large number of complete Fresnel zones take part in the reradiation from the surface. (This approximation is not valid when the first Fresnel zones approach the shadowed part of the surface.)

We will define the time autocorrelation function $R(\tau)$ of $E_r(t)$ in terms of an ensemble average:

$$R(\tau) = \frac{1}{z_o}\left\langle E_r^*(t)\, E_r(t+\tau)\right\rangle \qquad (6.4)$$

where z_o is the free-space wave impedance. The dimension of $R(\tau)$ is power per unit area.

We can now combine Eqs. (6.3) and (6.4), which gives

$$R(\tau) \approx \frac{1}{z_o}\left(\frac{kE_t \cos\theta_o}{2\pi d_{or} d_{ot}}\right)^2 \left\langle \int_{-\infty}^{+\infty}\int_{-\infty}^{+\infty} \exp\{i[-\omega t + k(d_t + d_r)]\}\, d\xi_o\, d\eta_o \right.$$

$$\left. \int_{-\infty}^{+\infty}\int_{-\infty}^{+\infty} \exp\{i[\omega t + \omega\tau - k(d_t' + d_r')]\}\, d\xi_o'\, d\eta_o' \right\rangle \qquad (6.5)$$

Note here that the last double integral is not equal to the first double integral since the coordinate system used for the integration has moved during the time τ.

For the phase path in the last integral one can show that (since $d_{ot}, d_{or} >> \xi_o', \eta_o', h'$)

$$k(d_t' + d_r') \approx \left[d_{ot} + d_{or} + (\dot{d}_{ot} + \dot{d}_{or})\tau + \frac{\xi_o'^2}{2}\left(\frac{\cos^2\theta_o}{d_{or}} + \frac{\cos^2\theta_o}{d_{ot}} + \frac{2\cos\theta_o}{R_p}\right) + \frac{\eta_o'^2}{2}\left(\frac{1}{d_{or}} + \frac{1}{d_{ot}} + \frac{2\cos\theta_o}{R_p}\right) + 2h'\cos\theta_o \right] k \qquad (6.6)$$

where $\dot{d}_{ot}$ and $\dot{d}_{or}$ denote the time rate of change of d_{ot} and d_{or}, respectively.

Combining Eq. (6.5) and Eq. (6.6), one obtains:

$$R(\tau) \approx \frac{1}{z_o}\left(\frac{kE_t \cos\theta_o}{2\pi d_{or} d_{ot}}\right)^2 \exp\{i[\omega\tau - k(\dot{d}_{or} + \dot{d}_{ot})\tau]\} \int_{-\infty}^{+\infty}\int_{-\infty}^{+\infty}\int_{-\infty}^{+\infty}\int_{-\infty}^{+\infty}$$

$$\cdot \exp\left[i\,\frac{k}{2}\left(\frac{\cos^2\theta_o}{d_{or}} + \frac{\cos^2\theta_o}{d_{ot}} + \frac{2\cos\theta_o}{R_p}\right)(\xi_o^2 - \xi_o'^2)\right]$$

$$\cdot \exp\left[i \frac{k}{2} \left(\frac{1}{d_{or}} + \frac{1}{d_{ot}} + \frac{2 \cos\theta_o}{R_p} \right) (\eta_o^2 - \eta_o'^2) \right]$$

$$\cdot \left\langle \exp\left[i2k \cos\theta_o (h - h') \right] \right\rangle d\xi_o \, d\xi_o' \, d\eta_o \, d\eta_o' \qquad (6.7)$$

where

$$h = h(\xi_o, \eta_o, t)$$

$$h' = h(\xi_o', \eta_o', t + \tau)$$

The next step in this development consists of changing dummy variables of integration. To be more specific, what we want to do is to integrate in a coordinate system that is fixed to the surface instead of moving along with the Fresnel zone pattern, such as our present coordinate system does. We have already defined a useful coordinate system for this purpose in Fig. 36. This was the $\xi\eta\zeta$-coordinate system which coincides with the subscripted coordinate system ($\xi_o\eta_o\zeta_o$ system) at time t (see Fig. 36), but is fixed on the surface.

Let v_ξ and v_η be the velocity with which the center of the first Fresnel zone is moving over the surface in the ξ and η directions, respectively. Then we have at time t,

$$\xi = \xi_o \qquad \eta = \eta_o$$

and at time $(t + \tau)$,

$$\xi' = v_\xi \tau + \xi_o' \qquad \eta' = v_\eta \tau + \eta_o'$$

If we also introduce $\Delta\xi = \xi' - \xi$ and $\Delta\eta = \eta' - \eta$, we can use ξ, η, $\Delta\xi$, and $\Delta\eta$ as dummy variables of integration. This gives

$$\xi_o' = \xi + \Delta\xi - v_\xi \tau$$

$$\eta_o' = \eta + \Delta\eta - v_\eta \tau \qquad (6.8)$$

$$\left.\begin{aligned} \xi_o^2 - \xi_o'^2 &= (v_\xi \tau - \Delta\xi)(2\xi + \Delta\xi - v_\xi \tau) \\ \eta_o^2 - \eta_o'^2 &= (v_\eta \tau - \Delta\eta)(2\eta + \Delta\eta - v_\eta \tau) \end{aligned}\right\} \tag{6.9}$$

$$\text{and} \quad h - h' = h(\xi,\eta) - h(\xi + \Delta\xi,\ \eta + \Delta\eta) \tag{6.10}$$

We will now assume that h has a gaussian joint-probability density function. This gives

$$\left\langle \exp\left[i2k \cos\theta_o (h - h')\right] \right\rangle = \exp\left\{-4k^2 \overline{h^2} \cos^2\theta_o \left[1 - \rho\left(\sqrt{\Delta\xi^2 + \Delta\eta^2}\right)\right]\right\} \tag{6.11}$$

(The left side can be considered the joint characteristic function of the gaussian random variables h and h'. Expressions for the joint characteristic function of gaussian random variables can be found in most textbooks on the subject.)

In Eq. (6.11), $\overline{h^2}$ denotes the mean square height and $\rho\left(\sqrt{\Delta\xi^2+\Delta\eta^2}\right)$ is the normalized autocorrelation function for h. The mean of h is zero since we have chosen the mean planetary surface with radius R_p as the reference level.

We can now combine Eqs. (6.7), (6.8), (6.9), and (6.11), which gives:

$$R(\tau) \approx \frac{1}{z_o}\left(\frac{kE_t \cos\theta_o}{2\pi d_{or} d_{ot}}\right)^2 \exp\left\{i[\omega - k(\dot{d}_{ot} + \dot{d}_{or})]\tau\right\}$$

$$\int_{-\infty}^{+\infty}\int_{-\infty}^{+\infty} \exp\left\{-4k^2 \overline{h^2} \cos^2\theta_o \left[1 - \rho\left(\sqrt{\Delta\xi^2 + \Delta\eta^2}\right)\right]\right\}$$

$$\exp\left[-i\frac{k}{2}\left(\frac{\cos^2\theta_o}{d_{or}} + \frac{\cos^2\theta_o}{d_{ot}} + \frac{2\cos\theta_o}{R_p}\right)(v_\xi \tau - \Delta\xi)^2\right]$$

$$\exp\left[-i\frac{k}{2}\left(\frac{1}{d_{ot}} + \frac{1}{d_{or}} + \frac{2\cos\theta_o}{R_p}\right)(v_\eta \tau - \Delta\eta)^2\right]$$

$$\int_{-\infty}^{+\infty} \exp\left[ik\left(\frac{\cos^2\theta_o}{d_{or}} + \frac{\cos^2\theta_o}{d_{ot}} + \frac{2\cos\theta_o}{R_p}\right)(v_\xi\tau - \Delta\xi)\xi\right] d\xi$$

$$\int_{-\infty}^{+\infty} \exp\left[ik\left(\frac{1}{d_{ot}} + \frac{1}{d_{or}} + \frac{2\cos\theta_o}{R_p}\right)(v_\eta\tau - \Delta\eta)\eta\right] d\eta\ d(\Delta\xi)\, d(\Delta\eta) \tag{6.12}$$

The integrations in ξ and η yield δ functions. After integration also with respect to $\Delta\xi$ and $\Delta\eta$, one finds

$$R(\tau) \approx R(0)\exp\{i[\omega\tau - k(\dot{d}_{or} + \dot{d}_{ot})\tau]\} \exp\{-4k^2\,\overline{h^2}\cos^2\theta_o\,[1 - \rho(v\tau)]\} \tag{6.13}$$

where

$$v = \sqrt{v_\xi^2 + v_\eta^2} \tag{6.14}$$

and

$$R(0) \approx \frac{1}{z_o}\left(\frac{E_t}{d_{or}d_{ot}}\right)^2 \frac{\cos\theta_o}{\left(\frac{\cos\theta_o}{d_{or}} + \frac{\cos\theta_o}{d_{ot}} + \frac{2}{R_p}\right)\left(\frac{1}{d_{or}} + \frac{1}{d_{ot}} + \frac{2\cos\theta_o}{R_p}\right)} \tag{6.15}$$

Equation (6.13) shows that by measuring $R(\tau)$ we can determine $\rho(v\tau)$ if the rest of the parameters are known.

We see that $\overline{h^2} = 0$ gives a doppler shift of the reflected signal but no frequency broadening. However, we are not interested in smooth spheres but in rough planets. For $\overline{h^2} \gg \lambda^2$ one has the situation illustrated in Fig. 38, where it is assumed that the derivative of $\rho(v\tau)$ exists for $v\tau = 0$, and that for small $(v\tau)$:

$$\rho(v\tau) \approx 1 - \left(\frac{v\tau}{L}\right)^2 \tag{6.16}$$

This gives

$$R(\tau) \approx R(0)\exp\{i[\omega - k(\dot{d}_{or} + \dot{d}_{ot})]\tau\} \exp\left[-4k^2\,\overline{h^2}\cos^2\theta_o\left(\frac{v\tau}{L}\right)^2\right] \tag{6.17}$$

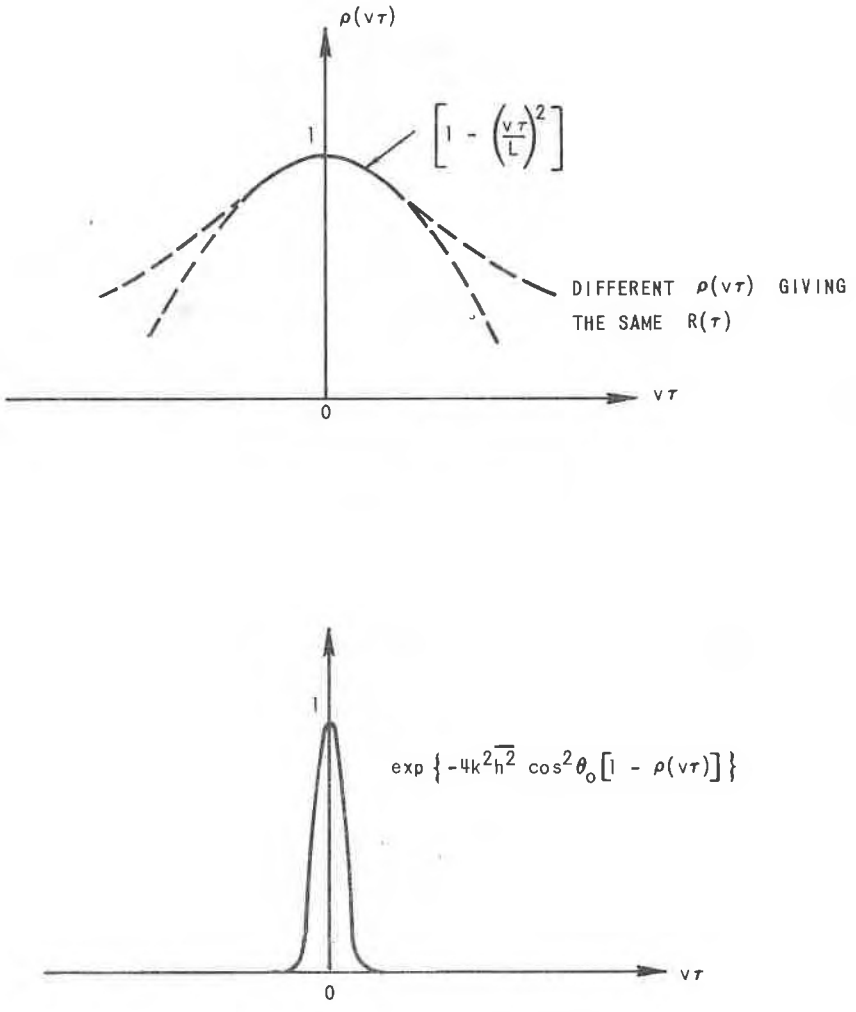

FIG. 38. SURFACE AND SIGNAL AUTOCORRELATION FUNCTIONS.

In this case we see that it really does not make any difference what shape $\rho(v\tau)$ has far away from the origin as long as it is less than 1. The reason is that the factor $(4k^2\ \overline{h^2}\ \cos^2\theta_o)$ has such a large value that $R(\tau)$ for practical purposes is zero, unless $\rho(v\tau)$ is very close to 1. Under these conditions we can only hope to determine $\rho(v\tau)$ from $R(\tau)$ for small values of the argument, and this may not be enough to draw conclusions about surface-roughness components with larger scales.

B. SPECTRAL BROADENING OF THE REFLECTED SIGNAL

Equation (6.17) gives, for the power spectral density of the reflected signal,

$$S(f) \approx \frac{\lambda L R(0)}{4\sqrt{\pi\ \overline{h^2}}\ v\ \cos\ \theta_o}\ \exp\left[-\frac{1}{\overline{h^2}}\left(\frac{cL}{4v\ \cos\ \theta_o}\right)^2\left(1 - \frac{f}{f_c}\right)^2 \right] \qquad (6.18)$$

where

$$f_c = \frac{\omega}{2\pi} - \frac{1}{\lambda}\left(\dot{d}_{ot} + \dot{d}_{or}\right)$$

= center frequency in the spectrum of the reflected signal

c = free-space phase velocity

λ = free-space wavelength at the center frequency

L = horizontal scale parameter for the surface irregularities

θ_o = angle of incidence at the center of the first Fresnel zone

v = the velocity with which the center of the first Fresnel zone is moving across the planetary surface.

The power spectrum takes on other shapes for other values of $\overline{h^2}$. For $\overline{h^2}$ equal to zero, the spectrum becomes a δ function; and for intermediate values of $\overline{h^2}$, one can find an expansion for the spectrum containing a δ function plus an infinite series [Ref. 14]. The power associated with the δ function has been assumed negligible in Eq. (6.18).

Finally we obtain the rms bandwidth of the spectrum from Eq. (6.18):

$$2\Delta f = 4\sqrt{2\ \overline{h^2}}\ f_c\ \frac{v\ \cos\ \theta_o}{cL} \qquad (6.19)$$

The rms bandwidth of the reflected signal can also be found directly from Eq. (6.13) without first assuming that $\overline{h^2} \gg \lambda^2$, and that $\rho(v\tau)$ for small arguments is given by Eq. (6.16). Assuming again that the initial slope of $\rho(v\tau)$ is zero, one obtains:

$$2\Delta f = f_c \frac{4v \cos \theta_o}{c} \left[- \overline{h^2} \left(\frac{d^2 \rho(x)}{dx^2} \right)_{x=0} \right]^{1/2} \tag{6.20}$$

C. THE RADAR CROSS SECTION (σ_r) OF THE PLANET

The average reflected power per unit area at the spacecraft is $R(0)$, given by Eq. (6.15). Since $1/d_{ot}$ is negligible compared to $1/d_{or}$ and $2/R_p$, we have

$$R(0) \approx \frac{1}{z_o} \left(\frac{E_t}{d_{ot}} \right)^2 \frac{\cos \theta_o}{\left(\cos \theta_o + \frac{2d_{or}}{R_p} \right) \left(1 + \frac{2d_{or} \cos \theta_o}{R_p} \right)} \tag{6.21}$$

We can now relate $R(0)$ to the radar cross section σ_r of the planet. Here the radar cross section will be defined so that σ_r times incident power per unit area on the planet gives a power which, if scattered isotropically, would give the time average power per unit area $R(0)$ reflected to the receiver. Thus

$$R(0) = \frac{1}{z_o} \left(\frac{E_t}{d_{ot}} \right)^2 \frac{\sigma_r}{4\pi r_s^2} \tag{6.22}$$

where r_s is the distance between the spacecraft and the planet's center. Figure 39 shows how the normalized radar cross section varies with r_s/R_p and θ_o. The limiting cases $r_s/R_p = 1$ and $r_s/R_p = \infty$ correspond to reflection from a plane and a distant sphere, respectively. Figure 40 shows the same result as a function of α, which here is the angle between the transmitter and the receiver as viewed from the center of the planet.

It is of interest to check the results derived here by introducing $\overline{h^2} = 0$ and comparing it with the expressions one can derive for a

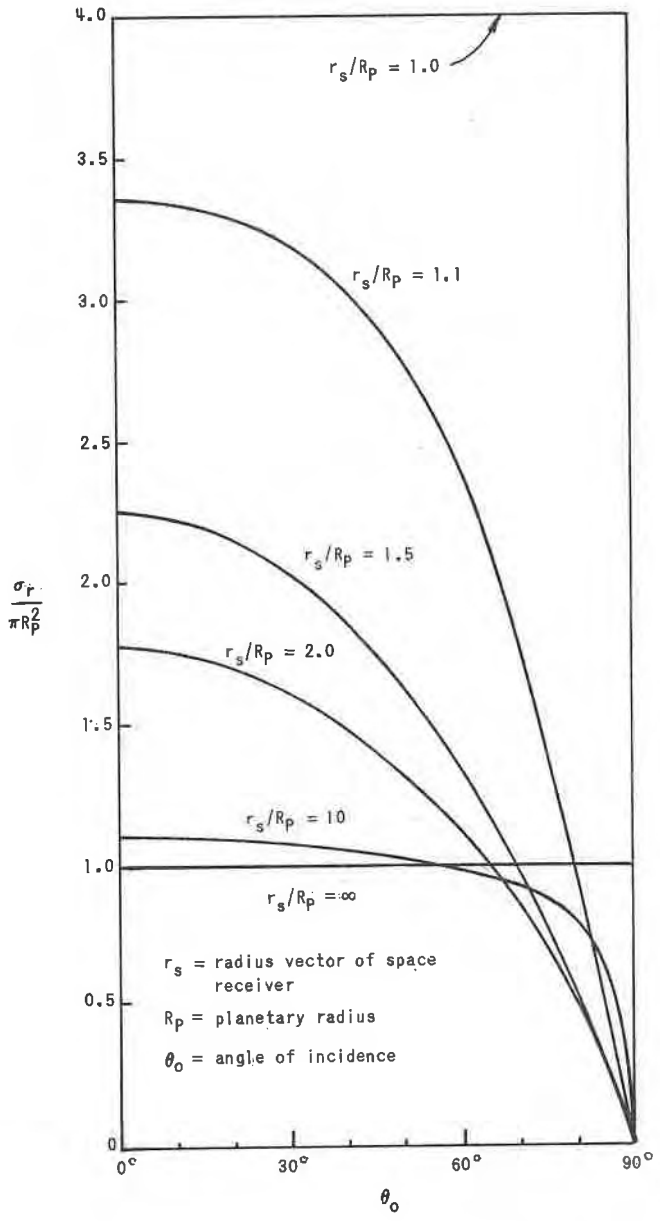

FIG. 39. RADAR CORSS SECTION OF THE PLANET VS r_s/R_p AND θ_o.

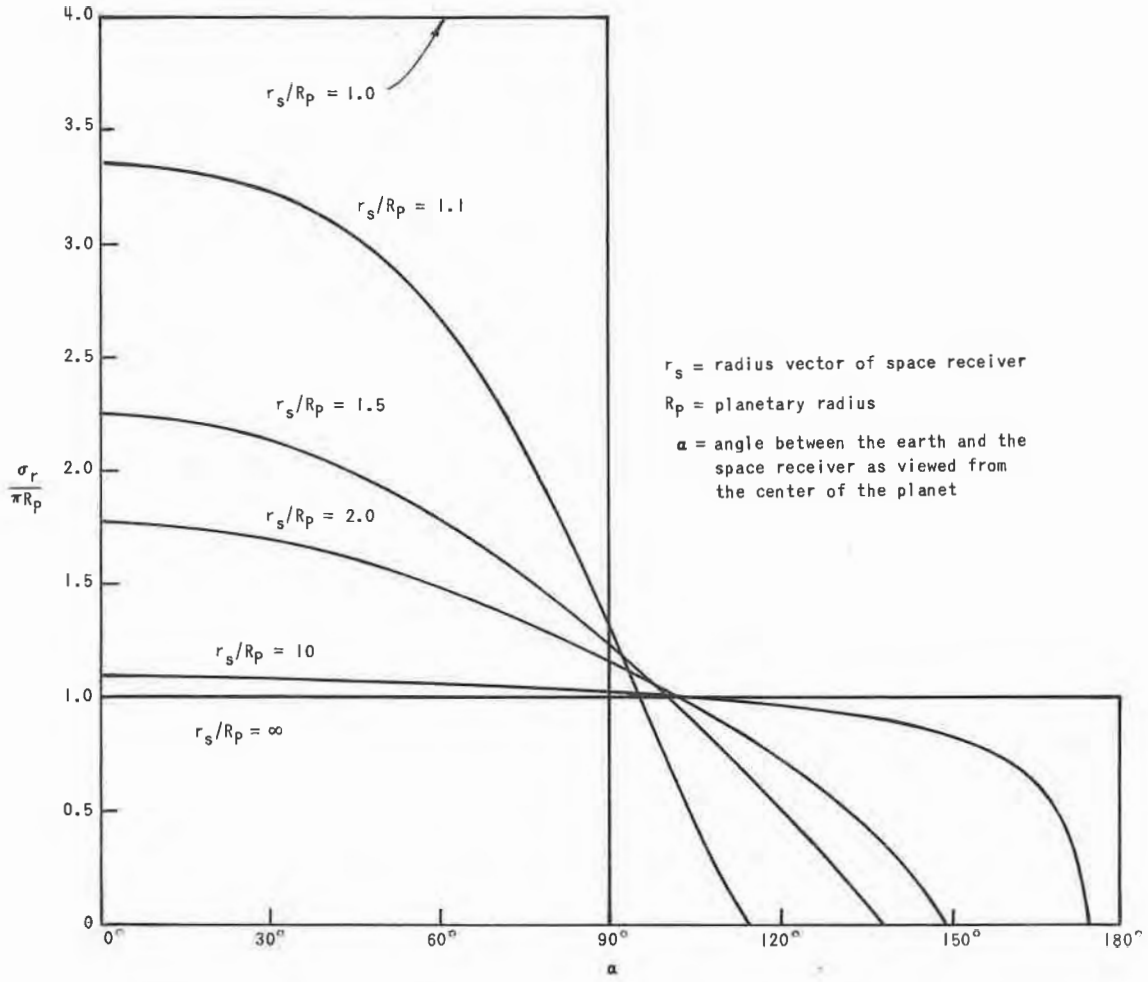

FIG. 40. RADAR CROSS SECTION OF THE PLANET VS r_s/R_p AND α.

smooth conducting sphere. We notice the σ_r does not depend on $\overline{h^2}$ at all, at least not to the degree of approximation used here. This lack of dependence must mean that the σ_r derived here is the same as for a smooth conducting sphere. Comparison with expressions obtained earlier for this case shows that this is indeed true [Ref. 15].

We assumed that the entire surface was illuminated when we applied the Huygens-Kirchhoff principle. This assumption is no longer true for large θ_o because part of the surface will then lie in the shade of hills and mountains. This shadowing will tend to reduce σ_r for large values of θ_o.

So far we have assumed that the surface is a perfect reflector. It is necessary to multiply the radar cross section found above with the power reflection coefficient when only part of the power is reflected.

D. NUMERIC EXAMPLE

A numeric example may be helpful in order to understand the problem better. Figure 41 shows the hyperbolic trajectory for a spacecraft flying by Venus.

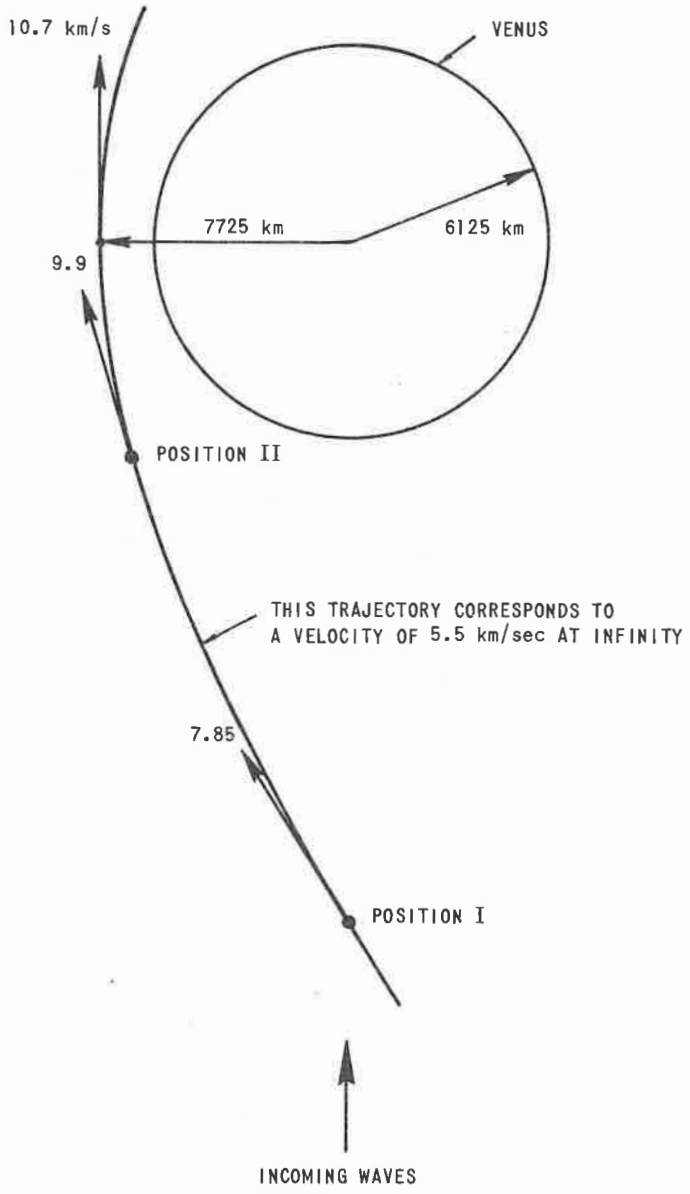

FIG. 41. ASSUMED FLY-BY TRAJECTORY.

We shall first compare the power received from the reflected wave and the direct traveling wave. The power received directly from the earth (P_d) is given by

$$P_d = \frac{P_t}{4\pi} g_T \frac{A_{rd}}{D^2} \tag{6.23}$$

where P_t = transmitted power

g_T = transmitter gain toward Venus

A_{rd} = receiving aperture directed toward the earth

D = distance between Venus and the earth.

For the power received from Venus (P_r), we have:

$$P_r = \frac{P_t}{4\pi} g_T \frac{\sigma_r}{D^2} \frac{A_{rr}}{4\pi r_s^2} \tag{6.24}$$

where A_{rr} = receiving aperture toward Venus

r_s = distance between the spacecraft and the center of Venus

σ_r = the radar cross section of Venus as viewed from the spacecraft. A power reflection coefficient of 0.1 will be used for the surface on Venus.

Assuming that $A_{rr} = A_{rd}$, we find

$$\frac{P_r}{P_d} = \frac{\sigma_r}{4\pi r_s^2} \tag{6.25}$$

At positions I and II in Fig. 41, this gives

$$10 \log \frac{P_r}{P_d} = \begin{cases} -25.4 \text{ db} & \text{(position I)} \\ -17.0 \text{ db} & \text{(position II)} \end{cases}$$

We see that the total power reflected from the planet is way below the power in the direct signal even though the receiver is passing by close to the surface on Venus.

The spectra are computed from Eq. (6.18) and shown in Fig. 42. It has been assumed here that the waves from the earth have a frequency of 50 Mc in the Venus frame and $\sqrt{\overline{h^2}}/L$ has been set equal to 1/10.

It is necessary to specify some more of the parameters involved before we can estimate the signal-to-noise ratio for the reflected wave. Let

$$P_t = 400 \text{ kw}$$

$$g_T = 360$$

$$g_r = 1.4$$

$$D = 6 \cdot 10^{10} \text{ meters.}$$

These values give, for the average reflected power received at the spacecraft,

$$P_r = \begin{cases} 0.366 \cdot 10^{-16} & \text{w} \quad \text{(position I)} \\ 2.594 \cdot 10^{-16} & \text{w} \quad \text{(position II)} \end{cases}$$

From Eq. (6.18) one can now find the maximum power spectral density:

$$S(f_c) \approx \begin{cases} 0.474 \cdot 10^{-18} & \text{w/cps (position I)} \\ 0.55 \cdot 10^{-18} & \text{w/cps (position II)} \end{cases}$$

The total power received is increased as the spacecraft moves from position I to position II, but the rms bandwidth of the spectrum is increased too; as a result, the maximum power spectral density $S(f_c)$ is only slightly increased in this example.

Assuming a constant noise temperature of 6000 °K, one finds for the noise power spectral density N

$$N = kT = 8.275 \cdot 10^{-20} \text{ w/cps}$$

This gives the signal-to-noise ratio:

$$10 \log \frac{S(f_c)}{N} \approx \begin{cases} 7.58 \text{ db} & \text{(position I)} \\ 8.22 \text{ db} & \text{(position II)} \end{cases}$$

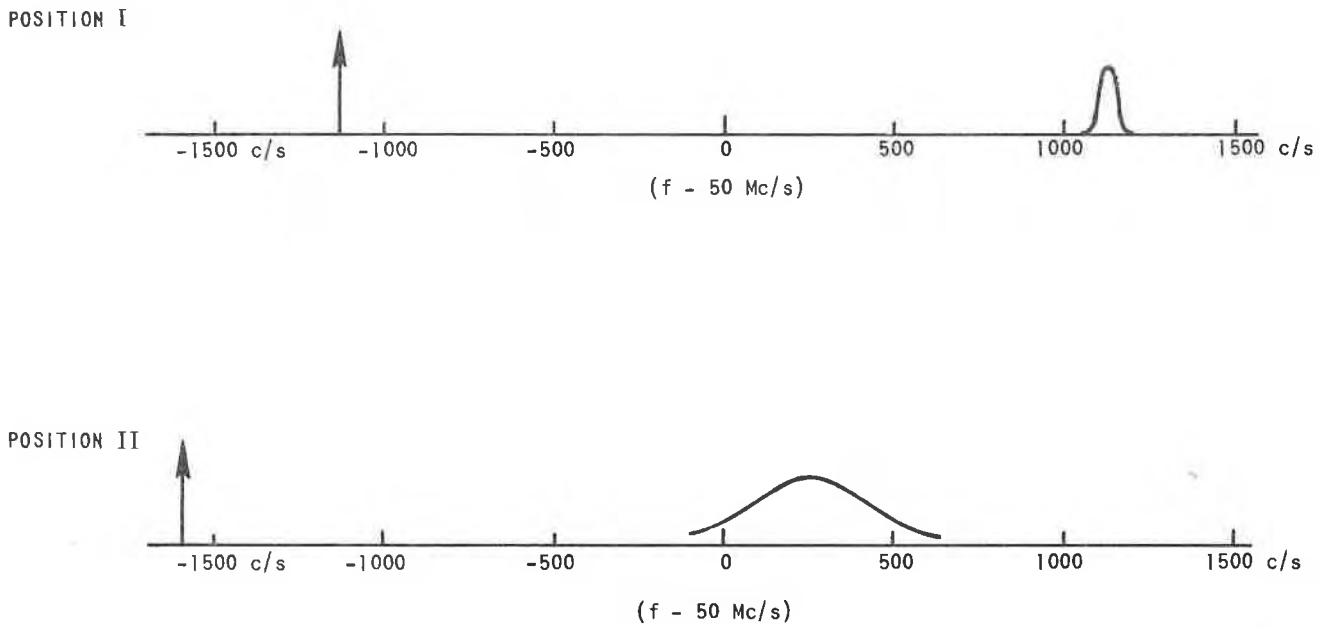

FIG. 42. POWER SPECTRA OF DIRECT AND REFLECTED SIGNAL.

which is proportional to $L/\sqrt{\overline{h^2}}$. The above signal-to-noise ratios are computed assuming $L/\sqrt{\overline{h^2}} = 10$. With $L/\sqrt{\overline{h^2}} = 4$ one would get a reduction in the signal-to-noise ratio by 4 db, while 20 would give 3 db increase in the signal level.

The power reflection coefficient in this numeric example was set equal to 0.1 for both receiver position I and receiver position II. That the reflectivity is considered equal in the two cases is just a simplifying assumption, since both the angle of incidence (θ_o) and the surface material of the reflecting areas may be different. We will come back to this problem in the next section.

As we have seen, the signal reflected from Venus contains information on the surface correlation function for the areas from which the signal is reflected. By observing the reflected signal over a large part of the orbit, one may determine how inhomogeneous the surface is and may find planes and mountain terrain. The bistatic-radar experiment may therefore offer a unique way of exploring the cloud-covered surface on Venus.

E. THE POLARIZATION OF RADIO WAVES REFLECTED FROM PLANETARY SURFACES AND ITS RELATION TO THE ELECTROMAGNETIC PROPERTIES OF THE SURFACE MATERIAL

We saw in the previous sections how to relate the fading of the reflected signal to the surface roughness. In this section we shall briefly look into how the polarization of the reflected wave can be related to the electromagnetic properties of the surface material.

We will assume that a circularly polarized wave is transmitted from the earth. The plane containing the transmitter, the planetary center, and the receiver will be called the plane of incidence. This is the $\zeta_o\xi_o$-plane in Fig. 36. We shall denote the electric field components of the reflected wave, E_{ri} and E_{rp}. Here E_{ri} is the electric field in the plane of incidence and E_{rp} is the field perpendicular to the plane of incidence.

The surface reflection coefficients are different for the two components of the wave. By comparing the rms value of E_{ri} with the field of the direct traveling wave, one can estimate the reflection

coefficient for this wave component. We have to make use of the approximation found for the radar cross section of a rough planet in order to find the absolute values of the reflection coefficients. This source of inaccuracy can be avoided if one instead considers the complex ratio (R):

$$R = \frac{E_{ri}}{E_{rp}} \exp\left(\pm i \frac{\pi}{2}\right) \qquad (6.26)$$

In general, both E_{ri} and E_{rp} are complex numbers. The sign in the exponent is chosen so that R is equal to the ratio between the reflection coefficients for the two wave components.

We will assume that the effects of small-scale roughness and multiple reflections are negligible.

The conductivity σ and the relative dielectric constant ϵ_r may vary over that part of the surface which is contributing to the echo. Assuming that the distribution in σ and ϵ_r is sufficiently narrow, one can show that their mean $\bar{\sigma}$ and $\bar{\epsilon}_r$ are given by:

$$\bar{\epsilon}_r - i \frac{\bar{\sigma}}{\omega \epsilon_o} \approx \sin^2\theta_o \left[1 + \tan^2\theta_o \left(\frac{R + 1}{R - 1}\right)^2\right] \qquad (6.27)$$

where $i = \sqrt{-1}$ and ϵ_o = dielectric constant of free space. The relative magnetic permeability for the surface material has been set equal to 1.

The size of the polarization ellipse of the reflected wave (measured in volts/meter) will change rapidly due to the fading. However, the axis ratio and the orientation of the ellipse will only change due to changes in θ_o, $\bar{\sigma}$, and $\bar{\epsilon}_r$.

The method indicated here permits us to map $\bar{\sigma}$ and $\bar{\epsilon}_r$. However, the resolution will be relatively poor unless the spacecraft is passing close to the surface. For multiple-layer surfaces it would be necessary to use several frequencies in order to determine the different parameters.

VII. CONCLUSIONS

In this study we have shown that bistatic radar may be used to explore planetary ionospheres and surfaces.

Transmitting radio waves from the earth and receiving them in a spacecraft that is moving behind a planet makes it possible to observe the variations in amplitude, phase path, or group path caused by the planetary ionosphere. It is shown that measurement of either the amplitude, the phase path, or the group path may be used to determine the radial electron density distribution in that part of the planetary ionosphere which is probed by the signal. However, it may be an advantage to do a couple of these measurements simultaneously in order to reduce possible uncertainties due to changes in the interplanetary medium or the earth's ionosphere during the experiment. The two radial electron density distributions obtained from the measurements during immersion and emersion are again related to the atmosphere on the planet. This relationship will also help us to make a better atmospheric model. The lower atmosphere may also be studied by using so high a frequency that the signal is only influenced by the atmosphere. Besides being of scientific interest, this information will be of vital importance if it is decided to land vehicles on the planet.

We have also shown that the statistical properties of the signal reflected from a planetary surface can be related to the surface statistics. It was shown, for instance, that the surface autocorrelation function can be related to the time autocorrelation function for the reflected signal when the surface-roughness scale is larger than the wavelength. This represents a generalization of results obtained previously for monostatic radar. We have also shown that the mean value for the dielectric constant and the conductivity can be found from the shape and orientation of the polarization ellipse for the reflected signal (assuming that a circularly polarized wave is transmitted). This method may find useful application in exploring Venus, where the surface is covered to a large extent by clouds.

APPENDIX A. WAVE-THEORY MODIFICATIONS CLOSE TO CAUSTICS AND SHADOW BOUNDARIES

The ray theory is not adequate along caustics and shadow boundaries. In these regions the propagation can be studied by means of Huygens' principle.

The caustic is the evolute of the wavefronts that have emerged from the planetary ionosphere. By making use of this relationship, one can find a convenient power series expansion for the phase of the signal. When maintaining terms up to the third power, one can express the fields around the caustic in terms of tabulated functions. This analysis was first worked out in optics by Airy, but the solution can also be found in books on radio-wave propagation [Ref. 16]. Although the geometry may appear to be somewhat different, the solution takes on the same form and the derivation is therefore not repeated here. The analysis shows a finite increase in the amplitude as the caustic is crossed.

The fields along a shadow boundary can also be determined from the wave theory. Here the solution can be expressed in terms of the Fresnel integrals, assuming that it is sufficient to maintain terms up to the second power in the expansion for the phase. The result is the same as for diffraction around an opaque straight edge (assuming that the reflected signal is negligible and that the straight-edge approximation applies), but one must take into account the fact that the ionosphere and the atmosphere will change the apparent position of the transmitter as viewed by the receiver.

One can show that the amplitude $E(x,y)$ as a function of receiver position x,y can be approximated by:

$$E(x,y) \approx$$

$$\left[\frac{k}{\pi}\left(\frac{1}{D}+\frac{1}{y}\right)\right]^{1/2} \int_{r_o=R_p}^{+\infty} \exp\left\{-i\left[\frac{k}{2}\left(\frac{1}{D}+\frac{1}{y}\right)\left(r_o - x\,\frac{D}{D+y}\right)^2 - 2\pi s_2(r_o)\right]\right\} dr_o \qquad (A.1)$$

where a factor $\exp[i\omega t - ik(D + y)]$ has been omitted. Here, $s_2(r_o)$ is given by Eq. (2.22), k is the free-space wave number, r_o is the dummy variable of integration, D is the distance between the transmitter and the planet, and R_p is the radius of the planet (see Fig. 5). Equation (A.1) gives $(1 - i)$ for the amplitude before the occultation starts.

A numeric example is shown in Fig. 43. This figure shows amplitude vs miss distance at 2300 Mc (the telemetry frequency on the space-probe mission to Mars), 20,000 km behind Mars. Equation (2.17) is used for the refractive index, assuming negligible water vapor, $T = 200\ ^\circ K$, and $P = 20$ and 0 millibars, respectively. At 2300 Mc the effect of the ionosphere is negligible.

Equation (A.1) can be changed into a more convenient form when the perturbations on the wavefronts, caused by the atmosphere or the ionosphere, are small. In that case it is more economical to compute the difference in amplitude with and without the perturbing medium present. This calculation will converge faster. The amplitude without any perturbing medium present can be found from the Cornu's spiral.

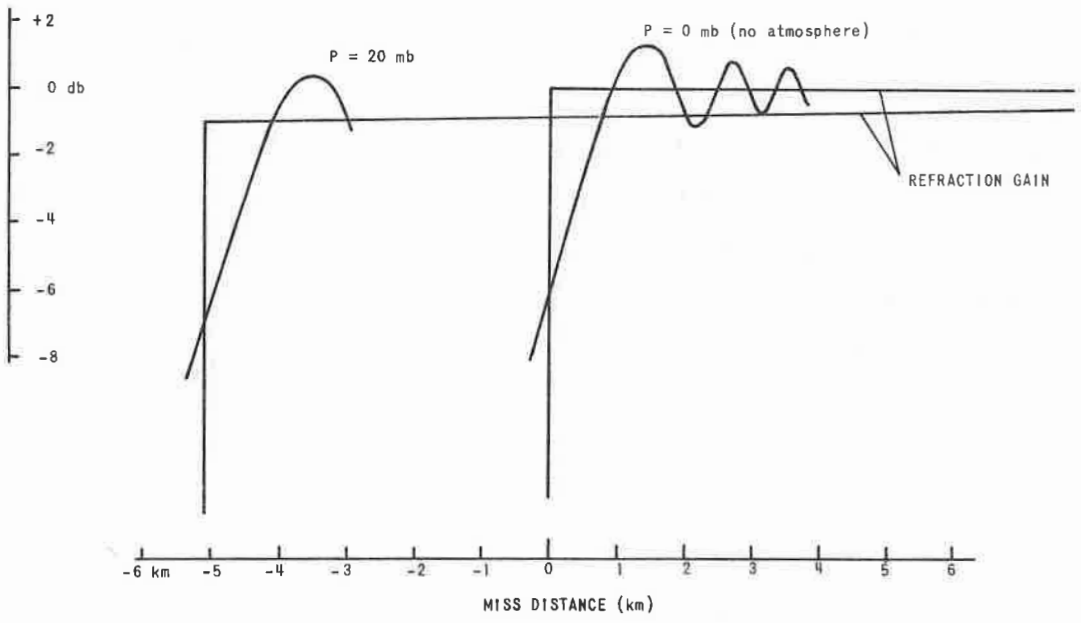

FIG. 43. AMPLITUDE VS MISS DISTANCE AT 20,000 km BEHIND MARS (f = 2300 Mc, H = 20 km, $T = 200^o$ K).

APPENDIX B. DETERMINATION OF THE ELECTRON DENSITY DISTRIBUTION BASED ON THE WAVE THEORY

Chapter V shows how one can determine the changes in the refractive index from measurement, for instance, of phase or amplitude during occultation. This analysis was all based on the ray theory. Equation (A.1) can also be inverted so as to give $s_2(r_o)$ (and therefore also the radial variation in the refractive index). This inversion gives:

$$s_2(r_o) =$$

$$\frac{1}{2\pi i}\,\ell n\left\{\frac{1}{y}\left[2\lambda\left(\frac{1}{D}+\frac{1}{y}\right)\right]^{-1/2}\int_{-\infty}^{+\infty} E(x,y)\,\exp\left[\,i\frac{k}{2}\left(\frac{1}{D}+\frac{1}{y}\right)\left(r_o - x\frac{D}{y+D}\right)^2\,\right]dx\right\} \tag{B.1}$$

for $r_o > R_p$, when y is independent of x. In this form the solution requires both amplitude and phase information.

REFERENCES

1. Max Born and Emil Wolf, Principles of Optics, Pergamon Press, New York, 1959.
2. F. G. Smith, J. Atmos. and Terr. Phys.,2, 1952, pp. 350-355.
3. J. L. Pawsey and R. N. Bracewell, Radio Astronomy, Oxford, 1955.
4. G. V. Evans and G. N. Taylor, Proc. Roy. Soc. A., 263, 1961, pp. 189-211.
5. V. R. Eshleman, P. B. Gallagher, and R. C. Barthle, "Radar Methods of Measuring the Cislunar Electron Density," J. Geophys. Res., 65, 1960, pp. 3079-3086.
6. S. Chapman, Proc. Phys. Soc., 43, pp.26-45.
7. G. F. Schilling, "A Note on the Atmosphere of Mars," J. Geophys. Res., 67, 1962, pp. 1170-1172.
8. J. A. Ratcliffe, The Magneto-ionic Theory and Its Applications to the Ionosphere, Cambridge University Press, Cambridge, 1959.
9. Georg Hamel, Integralgleichungen Einführung in Lehre und Gebrauch, Berlin, 1937.
10. F. B. Daniels and S. J. Bauer, "The Ionospheric Faraday Effect and its Applications," J. Franklin Inst., 267, 3, Mar 1959, pp. 187-200.
11. F. B. Daniels, "A Theory of Radar Reflection from the Moon and Planets," J. Geophys. Res., 66, 6, 1961, pp. 1781-1788.
12. A. Spizzichino, "Reflexion des ondes par la surface de la lune et des planetes considerée comme une surface irregulière," Rapport technique répertorié sous le no. 1235 CDS, 1962, distribué par le Service de Documentation Interministérielle du CNET, 38, Rue du Général Leclerc, Issy-les-Moulineaux, France.
13. T. Hagfors, "Some Properties of Radio Waves Reflected from the Moon and Their Relation to the Lunar Surface," J. Geophys. Res., 66, 3, 1961, pp. 777-785.
14. D. Middleton, An Introduction to Statistical Communication Theory, McGraw-Hill Book Co., New York, 1960, pp. 606-610.
15. B. van der Pol and H. Bremmer, "The Diffraction of Electromagnetic Waves from an Electrical Point Source round a Finitely Conducting Sphere, with Applications to Radiotelegraphy and the Theory of the Rainbow," Philosophical Mag., 24, 1937, pp. 825-863.
16. K. G. Budden, Radio Waves in the Ionosphere, Cambridge University Press, Cambridge, 1961.